

Topical Review

# Atomic and molecular data for spacecraft re-entry plasmas

R Celiberto<sup>1,2</sup>, I Armenise<sup>2</sup>, M Cacciatore<sup>2</sup>, M Capitelli<sup>2,3</sup>,  
F Esposito<sup>2</sup>, P Gamallo<sup>4</sup>, R K Janev<sup>5</sup>, A Laganà<sup>6</sup>,  
V Laporta<sup>2,7</sup>, A Laricchiuta<sup>2</sup>, A Lombardi<sup>6</sup>, M Rutigliano<sup>2</sup>,  
R Sayós<sup>4</sup>, J Tennyson<sup>7</sup> and J M Wadehra<sup>8</sup>

<sup>1</sup>Dipartimento di Ingegneria Civile, Ambientale, del Territorio, Edile e di  
Chimica, Politecnico di Bari, Bari, Italy

<sup>2</sup>PLASMI Lab, CNR NANOTEC, Bari, Italy

<sup>3</sup>Dipartimento di Chimica, Università degli Studi di Bari, Bari, Italy

<sup>4</sup>Departament de Química Física and Institut de Química Teòrica i  
Computacional, Universitat de Barcelona, Barcelona, Spain

<sup>5</sup>Macedonian Academy of Sciences and Arts, Skopje, Macedonia

<sup>6</sup>Dipartimento di Chimica Biologia e Biotecnologie, Università di Perugia,  
Perugia, Italy

<sup>7</sup>Department of Physics and Astronomy, University College London, London,  
UK

<sup>8</sup>Physics Department, Wayne State University, Detroit, MI, USA

E-mail: roberto.celiberto@poliba.it

November 2015

**Abstract.** The modeling of atmospheric gas, interacting with the space vehicles in re-entry conditions in planetary exploration missions, requires large set of scattering data for all those elementary processes occurring in the system. A fundamental aspect of re-entry problems is represented by the strong non-equilibrium conditions met in the atmospheric plasma close to the surface of the thermal shield, where numerous interconnected relaxation processes determine the evolution of the gaseous system towards the equilibrium conditions. A central role is played by the vibrational exchanges of energy, so that collisional processes involving vibrationally excited molecules assume a particular importance. In the present paper, theoretical calculations of complete sets of vibrationally state-resolved cross sections and rate coefficients are reviewed, focusing on the relevant classes of collisional processes: resonant and non-resonant electron-impact excitation of molecules, atom-diatom and molecule-molecule collisions as well as gas-surface interaction. In particular, collisional processes involving atomic and molecular species, relevant to Earth (N<sub>2</sub>,O<sub>2</sub>,NO), Mars (CO<sub>2</sub>,CO,N<sub>2</sub>) and Jupiter (H<sub>2</sub>,He) atmospheres are considered.

PACS numbers: 52.20.-j, 31.50.Df, 31.15.xv, 34.35.+a, 34.80

*Keywords:* elementary processes, excited states, nonequilibrium plasmas

Submitted to: *Plasma Sources Sci. Technol.*

## 1. Introduction

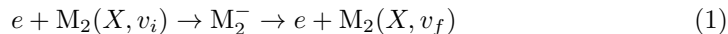
Exploring new frontiers in the planetary system means facing problems connected to the engineering design of thermal protection systems to shield any space vehicle from searing re-entry conditions, which are characterized by intense heat flux to the craft nose and the sharp increase of temperature in the shock region. High-enthalpy hypersonic flow experiments, performed by scaling down the problem in wind tunnel facilities, are used for testing new materials for the tiles, the diagnostics and the characterization of the parameters of the plasma generated during the atmospheric impact. On the other hand the computational fluid-dynamic rebuilding of those experiments gives an insight on the physics governing the plasma temporal and spatial evolution and can be thought of as providing a virtual laboratory for the control of conditions in realistic configurations. These models assume thermal (if not chemical) equilibrium on the belief that non-equilibrium effects play a minor role in every realistic case of interest but also to meet the requirement of computational efficiency. Attempts have been made to include non-equilibrium effects with multi-temperature approaches, integrating the detailed kinetics in different strategies, implementing macroscopic rate and multi-internal temperature models [1, 2, 3, 4]. However under strong non-equilibrium conditions the temperature can neither characterize the internal distributions, whose overpopulated tails significantly affect the chemical kinetics, nor describe the structures in the electron energy distribution function (eedf), resulting in large deviations of the kinetic rates for electron-impact induced processes from those obtained assuming a Maxwellian eedf. In this scenario the state-to-state (StS) approach [5, 6, 7, 8] can be considered the only reliable theoretical tool for the plasma modeling, self-consistently coupling the free-electron and chemical species collisional kinetics, and also including radiation models [9, 10, 11, 12] accounting for radiative processes entering the energy global balance. In this context we emphasize the role of radiation reabsorption by atoms and molecules in affecting the electron energy distribution function and therefore of macroscopic rates entering the kinetic approaches [12, 13, 14].

In StS models the chemical species in specific quantum states (electronically excited states, ro-vibrationally excited levels) are treated kinetically with independent master equations and characterized dynamically with state-specific cross sections and rate coefficients, with the reliability of the models and their predictive capability critically depending on the accuracy of the dynamical information [15, 16, 17]. Modern approaches in quantum molecular dynamics, combined with molecular beam experiments, has significantly enhanced and extended the knowledge of elementary process probabilities and a number of web-accessable databases, which collect and validate data, are now available to the modeling community [18, 19, 20]. Data set *completeness*, with respect to the vibrational ladder of ground electronic state, allows the implementation of full vibrational kinetics for atmospheric diatomic molecules, also including metastable states, but still retains approximations for the treatment of rotational levels, considered in equilibrium with the translation degree of freedom.

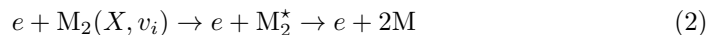
In aerospace applications, dealing with dissociation and ionization regimes [21, 22, 23, 24, 25, 26, 27, 28], a large number of elementary processes have to be included in the kinetic scheme, relevant to the main classes of electron-impact, heavy particle collisions and heterogeneous processes. The collision dynamics is investigated by adopting different theoretical approaches, from quantum to semi-classical, quasi-classical and also simplified classical or phenomenological methods, that offer the most favourable

balance between the level of approximation and the high computational load that usually characterize the calculation of complete sets, but avoiding the scaling laws commonly used [29, 30].

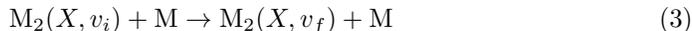
The processes promoted by electron impact on molecular target include vibrational and electronic excitations, dissociation and ionization, with progressively increasing energy threshold. In the framework of a StS approach the channels responsible for the vibrational pumping are of particular relevance, the most efficient being represented by the resonant vibrational excitation (RVE) mechanism



The resonant character of the process, with the temporarily formation of the negative molecular ion, determines the features of the energy profile of the cross section, the threshold position, ensuring the effectiveness of collisions with low-energy electrons and, for many chemical systems, the significant enhancement in cross section with the increasing initial vibrational quantum number [31, 32, 33, 34]. The negative ion can also evolve through alternative channels, leading to fragmentation, *i.e.* the dissociative electron attachment and the resonant dissociation [34, 35]. Dissociation actually can occur also through non resonant direct excitation of electronically excited states, either purely repulsive or non-radiatively coupled to repulsive states through predissociation mechanisms



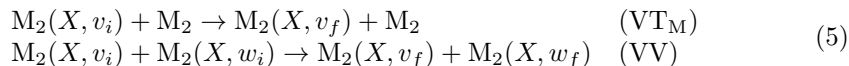
usually characterized by high-energy thresholds. These channels and the dependence of the cross sections on the vibrational quantum number of the molecular target have been investigated with semiclassical approaches [36, 37], as in the case of direct ionization of H<sub>2</sub>, O<sub>2</sub> and N<sub>2</sub> molecules [38, 39, 40, 41]. The dissociation mechanisms have been widely investigated due to their efficiency in affecting the vibrational distribution, either by destroying the vibrational energy content or also by forming atoms that are responsible of shaping the distribution tail through very effective vibrational deactivation in atom-molecule collisions (VT)



The dynamics of heavy-particle collisions on the relevant potential energy surface (PES) can be followed using the quasi-classical trajectory (QCT) method, which has proved to be accurate and compares well with quantum approaches. QCT provides a robust trajectory statistics, and allows the characterization of single- and multi-quanta transitions through vibrational analysis in both reactant and product channels [42, 43, 44, 45, 46, 47, 48, 49, 50, 51]. Rate coefficients are obtained with ro-vibrational resolution, but are usually included in kinetic codes as averages over the rotational distribution, which is assumed to be in equilibrium with the translation. Relying on the accuracy of the PES in the asymptotic regions, the QCT approach can be used also to estimate the probability of collisional induced dissociation

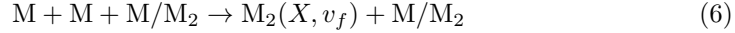


In molecule-molecule collisions the energy redistribution within the vibrational ladder operates through the VT<sub>M</sub> and VV processes



whose rates can be calculated in the framework of different theoretical approaches, including semiclassical [52, 53, 54, 55, 56] and quasiclassical trajectories [57], the forced-harmonic oscillator (FHO) [58, 59, 60] or the accurate close-coupled [61] methods. These approaches can also account for dissociation [59, 60, 62, 63].

Depending on the plasma conditions a recombination regime can favour the energy pumping preferentially at the top of vibrational ladder (three-body recombination)

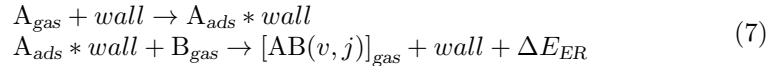


Recombination still represents a quite challenging process for direct dynamical investigation [64, 65]. However, in kinetic codes, usually the probability is derived, assuming microreversibility, through the principle of the detailed.

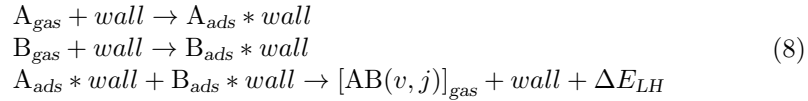
The interplay of these processes governs the plasma at a microscopic level in the gas-phase. However, it should be stressed that in realistic simulation of plasma systems the interaction of the plasma with the reactor walls or, in simulation of entry conditions, the recombination at the Thermal Protection System (TPS) wall, must be also considered. This interaction significantly affects the vibrational kinetics, due to both the formation of vibrationally excited molecules, through heterogeneous atomic recombination, or vibrational deactivation at the surface [66, 67, 68, 69, 70].

The three mechanisms commonly accepted for atom recombination at surfaces are:

- Eley-Rideal (ER) mechanism in which a species impinging from the gas-phase recombine with species previously adsorbed on the surface:



- Langmuir-Hinshelwood (LH) mechanism in which two adsorbed species in close sites on the surface recombine:



- Hot-Atom (HA) mechanism in which the impinging species becomes adsorbed but still possessing a high amount of energy. If this available energy is higher than the diffusion energy barriers, the adsorbed species could diffuse over the surface until they achieve adjacent sites that allow the final recombination of both adsorbed species [71].

The energy released in the recombination processes,  $\Delta E$ , depends critically on the recombination mechanism, on the surface site where the species is pre-adsorbed and, therefore, on the nature of the atomic adsorption (whether chemi- or physisorbed). The energy released in the reaction can be shared among the degrees of freedom of the newly formed molecules (rotations, vibrations, translation and, possibly, electronic) and the degrees of freedom of the substrate (phonons and, possibly, electrons).

Different systems of interest in aerospace applications have been investigated using Molecular Dynamics (MD) studies by means of classical or quasi-classical trajectories [72, 73, 74] and semiclassical methods [75, 76, 77, 78, 79, 80, 81, 82], by deriving the probability of recombination and the ro-vibrational nascent distributions.

The creation of a complete and consistent database of dynamical information for the StS modeling of re-entry non-equilibrium conditions, thus including all the

processes discussed so far for the relevant planetary atmosphere chemical species, could be considered as one of the challenging objectives of the fundamental research on elementary processes and as the essential prerequisite for any realistic attempt to use the StS models as a predictive tool.

This review offers a general overview of the information available to the modeling community, by focusing on molecular species relevant to Earth ( $\text{N}_2$ ,  $\text{O}_2$ ), Mars ( $\text{CO}_2$ ,  $\text{CO}$ ,  $\text{N}_2$ ) and Jupiter ( $\text{H}_2$ ,  $\text{He}$ ) atmospheres. It discusses the theoretical results and attempts to assess their accuracy by comparison with experiments, although the measurements of probabilities, for processes involving excited states, are quite scarce due to the difficulty in preparing beams of molecules in selected quantum states. Hydrogen plasmas, relevant for Jovian atmosphere, will be discussed: for these plasmas vast knowledge and experience have been accumulated by different communities interested in problems such as divertors and negative ion source plasmas studied within the thermonuclear fusion research [16, 83, 84, 85, 86, 87]. A specific section will be devoted to the  $\text{CO}_2$  system, which is attracting a renewed interest due to the relevance of  $\text{CO}_2$  plasmas in different technological applications to aerospace, energy and the environment [88, 89, 90]. The cross sections and rates for  $\text{CO}_2$  processes will be reviewed [91, 92, 93, 94] illustrating the complexity of constructing a vibrational kinetic model for a triatomic system [95].

## 2. Electron-molecule collisions

### 2.1. Non-resonant processes: vibronic excitation, dissociation and non-dissociative ionization

Reactive processes in electron-molecule collisions leading to dissociation and ionization can be regarded in the kinetic scheme as chemical source terms for atoms and electrons, significantly affecting the shape of the vibrational and electron distribution functions respectively. These non-resonant channels have been investigated, in the past, with simplified theoretical approaches, classical [96], semi-classical [97, 98, 99, 100] and phenomenological (BEf-scaling, *similarity approach*, Binary-encounter-Bethe model) [101, 102, 103, 39], offering a computationally cheap route to derive a complete set and a reasonable accuracy for the dynamical information when compared with experiments and quantum scattering theories.

The dissociation of  $\text{H}_2$ , induced by electron collisions, can be regarded as a benchmark, in fact the most efficient channel, represented by the dipole-forbidden excitation to the repulsive  $b^3\Sigma_u^+$  state, has been well studied. Cross sections from the ground  $v_i = 0$  level were estimated with accurate electron energy-loss spectroscopy (EELS) [104, 105, 106] and also the dependence on the initial vibrational level with different theoretical approaches, from the classical Gryzinski [38] to the quantum  $R$ -matrix [107, 108] and complex Kohn variational approach [109], were investigated. Figure 1(a) and (b) displays the energy profile, characterized by the near-threshold peak, showing also the expected shift in the threshold and a weak enhancement of the peak value for vibrationally excited molecules. General agreement is found among different approaches and for the  $v_i = 0$  theoretical results, mostly lying within the experimental uncertainties. Other channels contributing to global dissociation through predissociation mechanisms are, at relatively low-energies, the forbidden transitions to the first bound triplet states,  $a^3\Sigma_g^+$  and the metastable  $c^3\Pi_u$  [110]. It should be mentioned that the excitations involving triplets [112] are also of interest

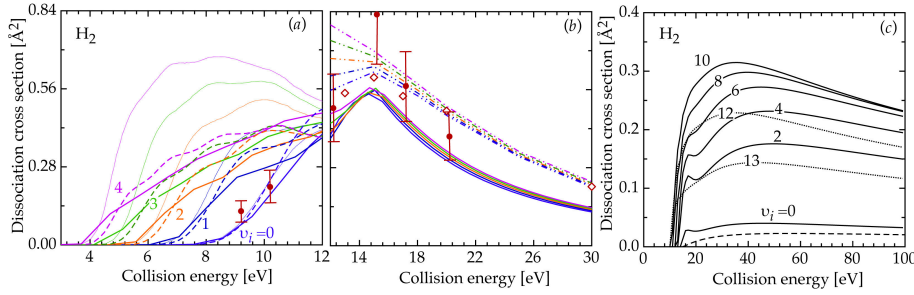


Figure 1: Dissociative excitation cross section of  $b^3\Sigma_u^+$  state in  $e\text{-H}_2$  collisions as a function of collision energy for different initial vibrational levels in (a) the threshold and (b) peak regions: solid lines [38], dashed-dotted lines [109], dotted lines [107], dashed lines [108]. Experimental results for  $v_i = 0$ : circles [105, 106], open diamonds [104]. (c) Direct dissociation cross section through singlets of  $\text{H}_2$  as function of collision energy for different initial vibrational levels [38, 110], compared for  $v_i = 0$  with Ref. [111].

in the kinetics, the Fulcher band ( $a^3\Sigma_g^+ \rightarrow d^3\Pi_u$ ) being relevant to diagnostics of vibrational temperature in plasma. Increasing the electron energy, high-threshold excitations of dipole-allowed singlet terms ( $B, B', B'' \ ^1\Sigma_u^+$  and  $C, D, D' \ ^1\Pi_u$ ) become accessible, these processes leading either to indirect vibrational pumping of the ground state through radiative decay (EV processes) [38], for excitations populating the discrete levels of the bound states, or to direct dissociation for transitions to the continuum of the electronically excited states. The theoretical direct dissociation cross sections, obtained using the semiclassical impact parameter method considering the contribution of all singlets [38, 110], are reported in Figure 1(c) showing the large enhancement of the broad high-energy maximum with increasing in the initial vibrational quantum number. The same figure compares the  $v_i = 0$  cross sections with recent results obtained by normalizing to the optical oscillator strength [111] and which predict values a factor two lower. With the further increase in electron energy, ionization processes are activated in  $e\text{-H}_2$  collisions. Dissociative and non-dissociative channels, proceeding through two different states of the molecular ion  $\text{H}_2^+$  ( $X^2\Sigma_g^+, ^2\Sigma_u^+$ ), have been studied within the classical approach [38, 110], deriving vibrationally-resolved cross sections and showing the dominant role of non-dissociative channel and the significant enhancement of ionization with the initial vibrational excitation of  $\text{H}_2$ . These results have been confirmed by recent calculations done in the same theoretical framework [113] and extended to consider ionizations initiated from electronically excited states.

Recently, direct dissociation cross sections for electron collisions with the  $\text{He}_2^+$  molecular ion have also been computed [114]. The calculations were performed for the electronic transition  $X^2\Sigma_u^+ \rightarrow A^2\Sigma_g^+$  starting from a given vibrational level of the ground state  $X$  and ending on the upper electronic state  $A$  whose potential curve is completely repulsive, so that dissociation occurs. The cross sections were calculated using the adiabatic nuclei approximation where the fixed-nuclei  $T$  matrices were obtained using the  $R$ -matrix method. The resulting cross sections show a low energy resonance peak, enhanced for vibrationally excited  $\text{He}_2^+$  ions. For higher incident electron energies a decreasing cross section trend is instead found with increasing the

vibrational excitation of the target.

Dissociation of  $N_2(X^1\Sigma_g^+)$  and  $O_2(X^3\Sigma_g^-)$  systems is mainly due to predissociation mechanisms following the excitations to bound excited states non-radiatively coupled with repulsive states. Cosby [115] gave experimental evidence of the large predissociation branching ratio in the vibronic excitation of singlet terms in the nitrogen energy diagram. Theoretical vibrationally-resolved cross sections have been obtained, using the classical Gryzinski method, for a number of excitation transitions ( $X^1\Sigma_g^+, \nu \rightarrow a^1\Pi_g, v' > 6; b^1\Pi_u; b^1\Sigma_u^+; c^1\Pi_u; c^1\Sigma_u^+; o^1\Pi_u; B^3\Pi_g, v' > 12; C^3\Pi_u, v' > 4$ ) involving both triplets and singlets states and, in a farther step, combined with predissociation probability for the derivation of a global dissociative cross section [36, 116]. Figure 2(a) demonstrates the significant dependence of the cross section on the initial vibrational quantum number, as well as, for the  $v_i=0$  curve, the agreement with experimental dissociation measurements [115]. The  $O_2$  dipole-allowed transition to the  $B^3\Sigma_u^-$  state, origin of the well-known Schumann-Runge bands and continuum in the spectrum, provides two electron-impact induced channels for dissociation through different mechanisms, *i.e.* the direct dissociation (Figure 2(b)) and the predissociation of vibrational level in the excited state (Figure 2(c)), whose cross sections, obtained in the semiclassical approach [37], show opposite trends with the initial vibrational excitation of the target. The most important process from the  $v_i = 0$  level is the dissociation to the continuum and while older experiments [117] agreed quite well with theoretical results, recent EELS measurements [118] seem to predict slightly lower values for the integral cross section. It is worth noting that the excited states mainly responsible

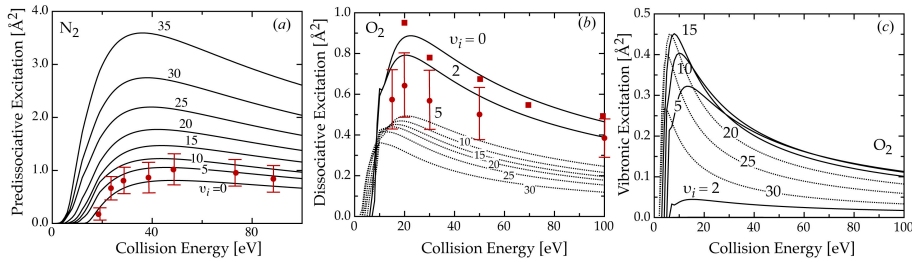


Figure 2: (a) State-specific global predissociation cross section in  $e$ - $N_2$  collisions as a function of collision energy for selected values of the initial vibrational quantum number [116, 36, 19], compared with experimental results for  $v_i = 0$  (markers) [115]. Dissociative excitation (b) and vibronic excitation (predissociation) (c) cross section in  $e$ - $O_2$  collisions in the Schumann-Runge transition [37] as a function of energy for different initial vibrational levels, compared with experimental results for  $v_i = 0$  [118] (circles) and electron-energy-loss experiments [117] (squares).

for predissociation, for both  $N_2$  and  $O_2$  systems, are also strongly affected by vibronic coupling effects, which lead to significant perturbations in the vibrational progression. The lowest three electronic terms of the  $^1\Sigma_u^+$  and  $^1\Pi_u$  spectroscopic series of  $N_2$  exhibit a mixed valence-Rydberg character [119, 120], while the valence  $O_2(B^3\Sigma_u^-)$  state is coupled with the  $E^3\Sigma_u^-$  Rydberg state, leading to resonances known as *longest band* (LB), and *second band* (SB) transitions [121, 122]. A reformulation of the similarity approach has recently been proposed to include, in a simple way, non-adiabatic effects. This was validated for of state-specific cross sections for  $N_2$  [91], where the results were shown to be in very good agreement with recent EELS experiments [123, 124].

Cross sections for non-dissociative ionization, induced by high-energy electron collisions, have been obtained for nitrogen [39, 40] and oxygen [41], extending the classical theory for atoms to diatomic molecule [39]. Principal channels from the ground state have been included according to the following ionization schemes:

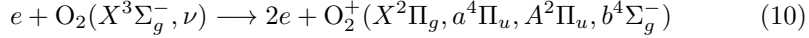
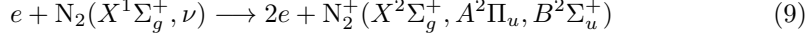


Figure 3(a) compares the total ionization cross section for  $\text{N}_2(v_i = 0)$  with experimental results [125, 126] and with values derived from experimental integrated electric dipole photoionization oscillator strengths [127]. Inspection of the vibrational profile for a selected value of the collision energy, in Figure 3(b), shows clearly the weak dependence on the initial vibrational excitation of the molecule, this behavior governed by the Franck Condon superposition of the initial and final vibrational levels. The partial ionization cross sections into different channels, reported in Figure 3(c),

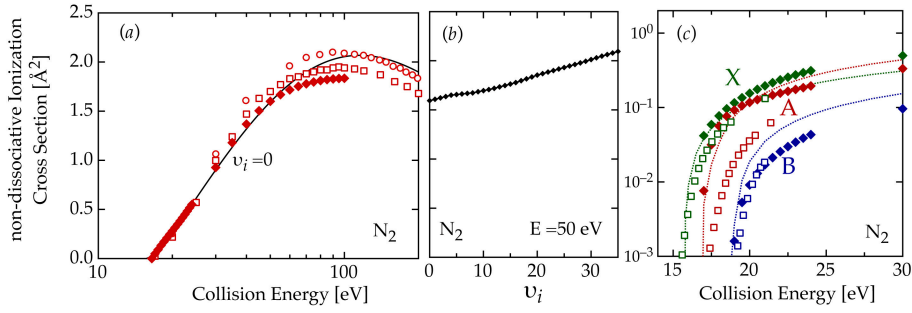
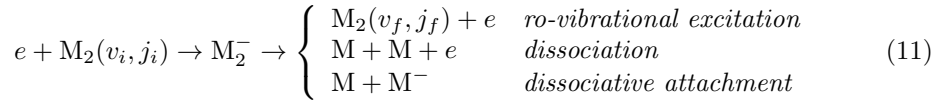


Figure 3: (a) Non-dissociative total ionization cross section of  $\text{N}_2$  as function of collision energy from  $v = 0$  vibrational level. (solid line) [40]; experimental results: (squares) [125], (circles) [126], (diamonds) [127]. (b) Vibrational profile of non-dissociative total ionization cross section at fixed collision energy. (c) Non-dissociative partial ionization cross sections as function of collision energy from  $v = 0$  vibrational level. (dotted line) [40]; (close diamonds) [127]; (open squares) [128].

demonstrate the agreement of classical estimation with the old Gryzinski [128] and recent results [127], also confirmed by the values of branching ratios,  $\eta_{X^2\Sigma_g^+}^{\text{theo}} = 0.301$ ,  $\eta_{A^2\Pi_u}^{\text{theo}} = 0.494$ ,  $\eta_{B^2\Sigma_u^+}^{\text{theo}} = 0.204$  [39, 40], well comparing with inferred estimates at 100 eV by Van Zyl & Pendleton [129] ( $\eta_{X^2\Sigma_g^+}^{\text{exp}} = 0.320 \pm 0.147$ ,  $\eta_{A^2\Pi_u}^{\text{exp}} = 0.535 \pm 0.112$ ,  $\eta_{B^2\Sigma_u^+}^{\text{exp}} = 0.145 \pm 0.017$ ). For the  $\text{O}_2$  system [41] the classical theory of ionization was able to predict the dominant role of the  $\text{O}_2^+(X^2\Pi_g)$  experimentally observed, and also absolute value of partial cross sections at 100 eV,  $\sigma_{X^2\Pi_g}^{\text{theo}} = 0.874 \text{ \AA}^2$ ,  $\sigma_{a^4\Pi_u}^{\text{theo}} = 0.474 \text{ \AA}^2$ ,  $\sigma_{b^4\Sigma_g^-}^{\text{theo}} = 0.183 \text{ \AA}^2$ , well reproducing the direct experimental estimates of Ref. [130],  $\sigma_{X^2\Pi_g}^{\text{exp}} = 0.922 \pm 0.184 \text{ \AA}^2$ ,  $\sigma_{a^4\Pi_u}^{\text{exp}} = 0.508 \pm 0.102 \text{ \AA}^2$ ,  $\sigma_{b^4\Sigma_g^-}^{\text{exp}} = 0.221 \pm 0.044 \text{ \AA}^2$ . However large discrepancies exist between branching ratios determined by the role of the  $A^2\Pi_u$  channel, experimentally found to be negligible.

## 2.2. Resonant processes: vibrational excitation, dissociation and dissociative attachment

Electron-molecule resonant collisions play an important role in the chemistry of atmospheric plasmas as they provide efficient channels for internal excitation or dissociation of molecules. The collision mechanisms, according to the well-known resonance model, is based on the temporary trapping of the projectile electron by the target such that the molecular anion thus formed (also called the resonant state) has a finite lifetime, during which the electron can autodetach, leaving behind either an excited molecule or a fully dissociated molecule when this is excited to a vibrational continuum. Electronic excitations can also occur through a resonant collision, but transitions among the ro-vibrational levels of the ground electronic states are of particular interest due to their fundamental role in the atmospheric gas kinetics. On the other hand, if the lifetime of the resonant state is sufficiently long, it can lead to dissociative electron attachment (DEA) forming a neutral atom and an atomic anion. If  $M_2$  represents a diatomic molecule, and  $v_i, j_i$  and  $v_f, j_f$  two ro-vibrational energy levels of the same electronic state one has, schematically,



where  $M_2^-$  is the molecular negative ion in a resonant electronic state,  $M$  is a neutral atom and  $M^-$  is a negative atomic ion. Cross sections for these resonant processes have been calculated and measured for many molecules relevant for atmospheric plasmas. Table 1 shows the resonant processes for the main species for which cross section data are presently available. All the diatomic molecules included in the table are initially in their ground electronic state. The second column shows the electronic term symmetry of the resonant states  $M_2^-$  involved in the process. For hydrogen molecule cross sections are available for resonant processes occurring through three resonant states two of which,  $X^2\Sigma_u^+$  and  $B^2\Sigma_g^+$ , arising from  $H_2$  valence states ( $X^1\Sigma_g^+$  and  $b^3\Sigma_u^+$ ) and a third Rydberg-excited state, of  $2^2\Sigma_g^+$  symmetry, generated from several excited states of the target molecule [131]. From a theoretical point of view, the first step for the cross section calculation is the computation, for a suitable range of internuclear distance  $R$ , of the potential energy curves,  $V(R)$  and  $V^-(R)$ , for the electronic states of both the stable and resonant molecular species  $M_2$  and  $M_2^-$  respectively, as well as the computation of the resonance width,  $\Gamma(R)$ , of the  $M_2^-$  unstable state, linked to its lifetime,  $\tau$ , by  $\tau(R) = \hbar/\Gamma(R)$ . While the potential curve for the target state,  $V(R)$ , can be obtained by means of standard electronic structure calculations, the adiabatic resonance potential  $V^-(R)$  (resonance energy positions) and the width  $\Gamma(R)$  must be calculated by solving the fixed-nuclei electron-molecule collision problem. Among the many methods developed in the years for treating the scattering event [153, 154, 155, 156], recently the  $R$ -matrix method has been widely used, for the collision systems of Table 1, to provide the above curves and widths necessary for nuclear motion studies of the resonant processes (see sec. 2.4). A brief account of this method is given in the next section.

REACTION	RESONANT STATES	$N_v$	Ref.
$e + \text{N}_2(\text{X}^1\Sigma_g^+; v, j) \rightarrow e + \text{N}_2(\text{X}^1\Sigma_g^+; v', j)$ $e + \text{N}_2(\text{X}^1\Sigma_g^+; v, j) \rightarrow e + \text{N}(^4\text{S}) + \text{N}(^4\text{S})$	$\text{N}_2^-(^2\Pi_g)$	59	[32, 34, 132] [34]
$e + \text{O}_2(\text{X}^3\Sigma_g^-; v, j) \rightarrow e + \text{O}_2(\text{X}^3\Sigma_g^-; v', j)$ $e + \text{O}_2(\text{X}^3\Sigma_g^-; v, j) \rightarrow \text{O}(^3\text{P}) + \text{O}^-(^2\text{P})$ $e + \text{O}_2(\text{X}^3\Sigma_g^-; v, j) \rightarrow e + \text{O}(^3\text{P}) + \text{O}(^3\text{P})$	$\text{O}_2^-(^2\Pi_g, ^2\Pi_u, ^4\Sigma_u^-, ^2\Sigma_u^-)$	42	[31, 32, 133, 134, 135] [35, 136] [35, 136]
$e + \text{NO}(\text{X}^2\Pi; v, j) \rightarrow e + \text{NO}(\text{X}^2\Pi; v', j)$ $e + \text{NO}(\text{X}^2\Pi; v, j) \rightarrow \text{N}(^4\text{S}) + \text{O}^-(^2\text{P})$	$\text{NO}^-(^3\Sigma^-, ^1\Delta, ^1\Sigma^+)$	54	[32, 137, 138] [137, 139, 140]
$e + \text{CO}(\text{X}^1\Sigma^+; v, j) \rightarrow e + \text{CO}(\text{X}^1\Sigma^+; v', j)$ $e + \text{CO}(\text{X}^1\Sigma^+; v, j) \rightarrow \text{C}(^3\text{P}) + \text{O}^-(^2\text{P})$ $e + \text{CO}(\text{X}^1\Sigma^+; v, j) \rightarrow \text{C}(^3\text{P}) + \text{O}(^3\text{P})$	$\text{CO}^-(^2\Pi)$	81	[33] [141, 142] [141]
$e + \text{H}_2(\text{X}^1\Sigma_g^+; v_i, j_i) \rightarrow e + \text{H}_2(\text{X}^1\Sigma_g^+; v_f, j_f)$ $e + \text{H}_2(\text{X}^1\Sigma_g^+; v_i, j_i) \rightarrow \text{H}(^2\text{S}) + \text{H}^-(^1\text{S})$ $e + \text{H}_2(\text{X}^1\Sigma_g^+; v_i, j_i) \rightarrow \text{H}(^2\text{S}) + \text{H}(^2\text{S}) + e$	$\text{H}_2^-(\text{X}^2\Sigma_u^+)$	15	[143, 144, 145] [146, 143, 147, 148, 149] [150]
$e + \text{H}_2(\text{X}^1\Sigma_g^+; v_i, j_i) \rightarrow e + \text{H}_2(\text{X}^1\Sigma_g^+; v_f, j_f)$ $e + \text{H}_2(\text{X}^1\Sigma_g^+; v_i, j_i) \rightarrow \text{H}(^2\text{S}) + \text{H}^-(^1\text{S})$ $e + \text{H}_2(\text{X}^1\Sigma_g^+; v_i, j_i) \rightarrow \text{H}(^2\text{S}) + \text{H}(^2\text{S}) + e$	$\text{H}_2^-(\text{B}^2\Sigma_g^+)$	15	[143] [143] [150]
$e + \text{H}_2(\text{X}^1\Sigma_g^+; v_i, j_i) \rightarrow e + \text{H}_2(\text{X}^1\Sigma_g^+; v_f, j_f)$ $e + \text{H}_2(\text{X}^1\Sigma_g^+; v_i, j_i) \rightarrow \text{H}(^2\text{S}) + \text{H}^-(^1\text{S})$	$\text{H}_2^-(^2\Sigma_g^+, \text{Rydberg state})$	15	[83, 91, 87] [84, 86, 151, 91, 152]

Table 1: The first column shows the list of the reactions considered in the text occurring, according to the general scheme in (11), through the anionic resonant states shown in the second column.  $N_v$  is the number of vibrational levels belonging to the ground electronic state of the neutral molecule. The last column reports some relevant theoretical and experimental references.

### 2.3. $R$ -matrix methods

The  $R$ -matrix method is a rather general scattering formalism [157] which has been heavily adapted for treating electron-molecule collision calculations [155]. The physical basis of the  $R$ -matrix method is the division of the electron collision space into two regions: an inner region in which the complicated electron interaction with the target is treated in full and an outer region where the electron is assumed to move simply in the long-range potential due to the target. This representation of the problem has considerable algorithmic [158] and computational advantages which are discussed in detail in the references cited above. In particular, it is only for the outer region that the calculation needs to be repeated as a function of collision energy which means that performing calculations for many energies is computationally efficient.

As we have seen in the previous section, one feature of electron collisions with molecules is the temporary trapping of electrons in quasi-bound states which give rise to resonances. Within the Born-Oppenheimer approximation, for each resonance energy position and a width can be extracted from the scattering calculations by a number of methods such as fitting the eigenphases of the collision [159] or analyzing the time-delay of the collision process [160]. For broad (short-lived) resonances it can be necessary to account for effects beyond the Born-Oppenheimer approximation by considering the energy dependence of the resonance; such calculations, based in the so-called *non local model* [161, 162], briefly discussed in the next session, are possible within the  $R$ -matrix method [163], but have not been found necessary for the studies reviewed here.

Figure 4 shows some examples of potential curves for the ground states and the resonant states (see Table 1) of CO, N<sub>2</sub> and H<sub>2</sub> molecules, as well as the corresponding widths, obtained by the  $R$ -matrix method.

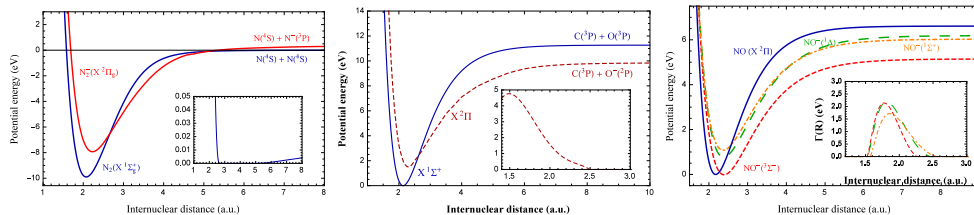


Figure 4: Potential energy curves for neutral and resonant states of  $N_2$ , CO and NO molecules. The small box in each panel shows the corresponding widths [34, 33, 32].

The ability to study electron scattering at a fine grid of energies means that resonances parameters can be mapped out in detail [164]. It is possible to look at highly-excited bound states in similar detail by performing scattering calculations at *negative collision energies* [165]; however the approach adopted for some of the system of Table 1 has largely been to use standard bound state molecular electronic structure codes such as MOLPRO [166] for such purposes.

#### 2.4. The role of nuclear dynamics in resonant processes

When an electron is trapped by a neutral N-electron molecule a resonant negative molecular ion is formed in a given electronic state and the nuclei motion takes place in the potential field,  $V^-(R)$ , of N+1 electrons. Quasi-bound ro-vibrational levels then arise which may decay through the channels represented in Eq. (11). From a theoretical point of view, if the resonant state is sufficiently stable, the Born-Oppenheimer separation of electrons and nuclei motions can be applied. This is the physical basis of the so-called *local complex potential model*, a theoretical description of the nuclei dynamics which provides the cross section expressions for the nuclear processes in (11). This model gives quite satisfactory results in many cases, and cross sections for many of the reactions listed in Table 1 have been obtained using this model. However, as already noted in the previous section, in cases of particular unstable resonant states, as for example that arising in electron- $H_2$  scattering, where the electron is trapped by the molecule by a centrifugal barrier and rapidly tunnels away, a more complete treatment of the electron-molecule collision, which goes to some extent beyond the Born-Oppenheimer approximation, is required such as that provided by the non-local model [156]).

#### 2.5. Resonant cross sections

Figure 5 (left panel) shows calculated local cross sections for resonant vibrational excitation in  $N_2$ , as a function of energy and for some initial vibrational level  $v_i$ , for one-quantum transitions ( $\Delta v_i = 1$ ). These transitions are usually characterized by quite large cross sections which means they play an important role in vibrational kinetics. The oscillatory structures in the cross sections is attributable to the quasi-bound vibrational wave functions of the resonant state. Figure 5 (right panel) displays the cross sections for resonant dissociation which show significant values for very high vibrational levels only [34]. These two processes occur, according to the mechanisms in Eq. (11), through the resonant state of symmetry  $^2\Pi_g$ , generated by the formation

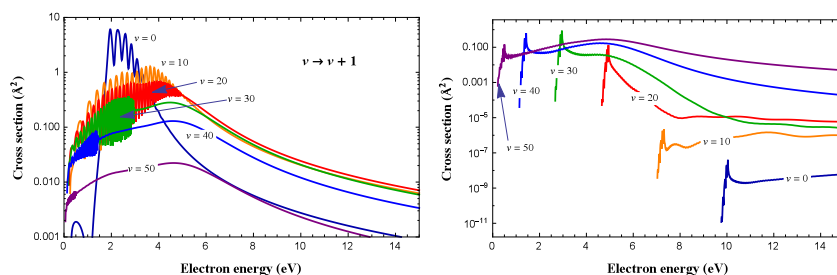


Figure 5: Electron-N<sub>2</sub> cross sections for one-quantum vibrational excitation and resonant dissociation [34].

of a centrifugal barrier (shape resonance). Dissociative attachment, instead, from this resonant state is not an allowed process as the atomic ion, N<sup>-</sup>, produced in the dissociation is unstable, owing to a positive electronic affinity [167, 168, 169]. Cross sections for the same resonant processes for O<sub>2</sub> molecule, including dissociative

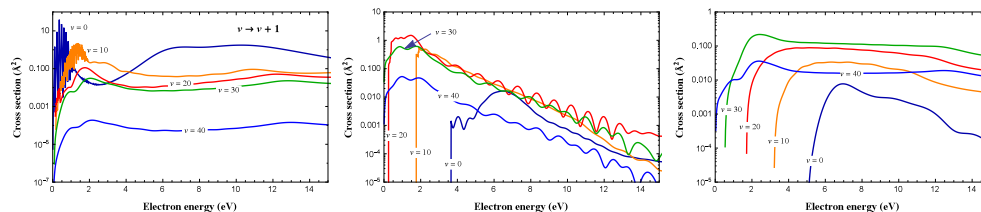


Figure 6: Electron-O<sub>2</sub> cross sections for one-quantum vibrational excitation, DEA and resonant dissociation [31, 35].

attachment, are shown in Figure 6. In this system, four resonant states (see Table 1), formed by adding the extra electron in one of the HOMO-LUMO molecular orbitals of the ground state configuration of the target molecule, contribute to the collision [31, 35]. Figure 7, finally, shows the cross sections for resonant one-quantum vibrational excitation [32] of nitric oxide molecule and dissociative attachment for some selected initial vibrational levels, the latter calculated using the non local model [137]. Also for this reactions three resonant states take part to the collision.

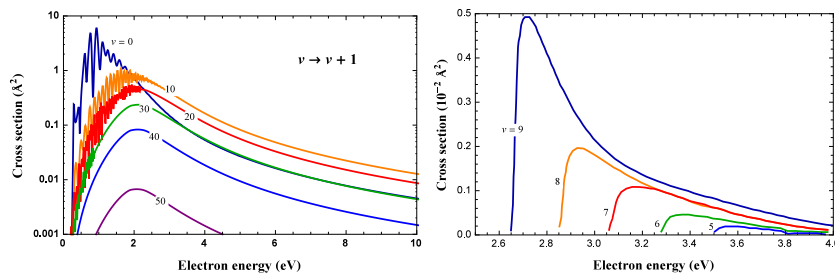


Figure 7: Left panel: Electron-NO scattering cross sections for one-quantum vibrational excitation [32] (left panel) and dissociative attachment for some initial vibrational level [137] (right panel).

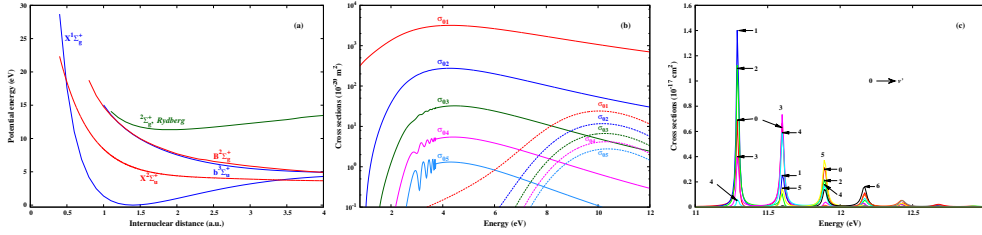


Figure 8: Panel (a): Potential energy curves for the  $\text{H}_2^-$  resonant states along with the  $X^1\Sigma_g^+$  and  $b^3\Sigma_u^+$  target states. Panel (b): Cross sections for the  $\text{H}_2$  vibrational excitation occurring through the  $X^2\Sigma_u^+$  and  $B^2\Sigma_g^+$  resonances [143]. Panel (c): Same process as in (b) but occurring through  $^2\Sigma_g^+$  Rydberg resonances [87].

For the CO molecule cross sections for vibrational excitation by electron impact, occurring through the resonant electronic state  $^2\Pi$  of Table 1, were calculated using the  $R$ -matrix potentials and widths shown in Figure 4 [33]. Recently, cross sections calculations were extended to the DEA and resonant dissociation processes, involving the above resonant state, as a function of the vibrational excitation of the molecule. The results are reported in Ref. [141].

Once the cross sections are known, rate coefficients for the resonant processes can be obtained if one assumes that in the plasma system electrons are found in thermal equilibrium. In this case the analytic Maxwellian energy distribution function can be used to average the collision cross sections. Calculated rate coefficients, which are of fundamental importance in kinetic modelings of plasmas, are now available for most of the reactions of Table 1 and can be found in the literature quoted in the same table.

The hydrogen molecule occupies a prominent place in the studies of resonant processes, both for the strong interest that it draws in many applicative areas and for its simplicity, which makes it suitable for investigations of the collision mechanisms and for testing theories. In the next section some historical results and recent developments are reviewed.

## 2.6. Resonant collisions involving $\text{H}_2$ molecule

In the range of energy from few eV to approximately 15 eV, three distinct resonant states of  $\text{H}_2^-$  (see Figure 8a) contribute significantly, each with its own characteristic peak behavior for various resonant processes. For electron energy between 2 eV and about 8 eV, the  $X^2\Sigma_u^+$  resonant state of  $\text{H}_2^-$  dominates all resonant processes. For energies between 8 eV and about 12 eV, the lowest excited  $B^2\Sigma_g^+$  state of  $\text{H}_2^-$  controls various resonant processes. For electron energies in the range from 11 eV to about 15 eV, the resonant processes are regulated by the  $^2\Sigma_g^+$  excited Rydberg electronic state of  $\text{H}_2^-$ .

The resonant vibrational excitation (RVE) cross sections  $\sigma_{v_i, v_f}$  of  $\text{H}_2$ , for the process occurring through the lowest two resonant states, are shown in Figure 8b. In this figure all the cross sections start from  $v_i = 0$ . Interestingly, near 10 eV, the RVE cross sections  $\sigma_{01}$  and  $\sigma_{02}$  are dominated by the  $X^2\Sigma_u^+$  state while the excitation of higher levels occurs predominantly through the  $B^2\Sigma_g^+$  state. The RVE cross sections, shown in Figure 8c for  $v_i = 0$ , are determined by the excited  $^2\Sigma_g^+$  Rydberg state of the molecular ion  $\text{H}_2^-$ . For each value of  $v_f$  these cross section shows multiple peaks

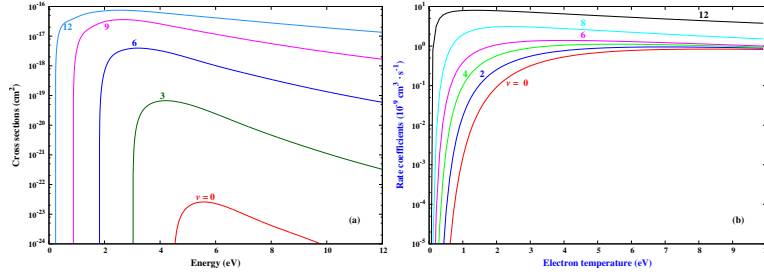


Figure 9: (a) Cross section for the resonant dissociation process [150] and (b) the corresponding rate coefficients as a function of the electron energy and temperature respectively.

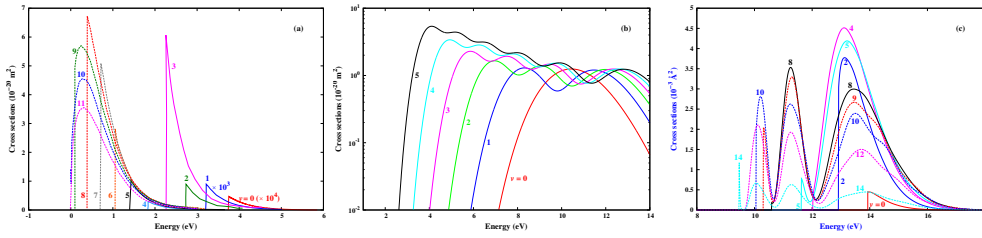


Figure 10: Dissociative electron attachment cross section occurring through the (a)  $X^2\Sigma_u^+$  [144], (b)  $B^2\Sigma_g^+$  [170] and (c)  $2\Sigma_g^+$  Rydberg state [151], as a function of the incident electron energy and for different  $v_i$ .

with the dominant peak shifting progressively to a higher energy as  $v_f$  is increased.

The two lowest resonant states of  $\text{H}_2^-$ ,  $X^2\Sigma_u^+$  and  $B^2\Sigma_g^+$ , contribute significantly to the dissociation of  $\text{H}_2$ . Because of the positioning of their potential energy curves, the  $X^2\Sigma_u^+$  resonance decays only to the continuum of  $\text{H}_2$  ground electronic state  $X^1\Sigma_g^+$ . The  $B^2\Sigma_g^+$  resonance, on the other hand, can decay to both the continua of  $X^1\Sigma_g^+$  and  $b^3\Sigma_u^+$  states of neutral  $\text{H}_2$ . Figure 9a illustrates the contribution of the  $X^2\Sigma_u^+$  resonance to the cross sections for dissociation of  $\text{H}_2$  for several different  $v_i$  and shows the strong cross section dependence on the initial vibrational level of the molecule. The peak value, in fact, increases by almost seven orders of magnitude as  $v_i$  increases, as already observed for  $\text{N}_2$  (see Figure 5b). On the other hand, contribution of the  $B^2\Sigma_g^+$  resonance to the dissociation cross sections (not shown) as a function of energy presents oscillatory behavior [150] and, for small values of  $v_i$ , its contribution to the dissociation cross sections becomes larger than the that of the  $X^2\Sigma_u^+$  resonance. No data are currently available for dissociation occurring through the Rydberg state. Figure 9b shows the *total* Maxwellian rate coefficients, *i.e.* the sum of all the above contributions to the  $\text{H}_2$  dissociation, as a function of average electron energy and for different levels  $v_i$ . For each level, the dissociation rates exhibits a broad maximum which increases rapidly as  $v_i$  is increased.

The shape of the DEA cross section depends on the nature of the  $\text{H}_2^-$  resonant state. For example, in the energy range below 5 eV, the  $X^2\Sigma_u^+$  resonant state contributes significantly to the DEA cross section. Furthermore, this cross section depends very sensitively on the initial vibrational energy of the neutral  $\text{H}_2$  molecule. This sensitivity can be appreciated in Figure 10a which shows DEA cross sections

as a function of electron energy for various values of  $v_i$  calculated using the nonlocal model approach [149, 144]. Figure 10b shows the cross sections for dissociative electron attachment to  $\text{H}_2$  proceeding through the formation of  $B^2\Sigma_g^+$  resonance. In this case, there is no significant enhancement of the DEA cross section, even if  $\text{H}_2$  molecule is initially vibrationally excited. Figure 10 c shows DEA cross sections as a function of electron energy, proceeding via the  $^2\Sigma_g^+$  Rydberg resonance, for different values of  $v_i$ . This state dissociates into  $\text{H}^-$  and an  $n = 2$  excited hydrogen atom. Interestingly, in this case there is not much enhancement of the cross section with increasing  $v_i$ . However, since the threshold for the DEA cross section is lowered as the vibrational level is increased, additional peaks of the cross section are revealed.

### 2.7. Further resonant processes

The electron-molecule reactions sketched in Eq. (11) do not exhaust all the possible resonant collisions. Associative detachment, for example, is also a resonant process which leads to molecular neutral species [171, 172]. It can be considered the inverse of dissociative attachment and its cross sections can be linked to the DEA ones by the principle of detailed balance.

Dissociative recombination is yet another process of great importance in plasma kinetics. This process involves a positive molecular ion,  $\text{M}_2^+$ , which after capturing the incident electron, can give rise to a neutral molecule in an unstable state toward electron re-emission. However, if the molecule is found in a repulsive state, typically a super-excited electronic state,  $\text{M}_2^*$ , or in a bound Rydberg state,  $\text{M}_2^*$ , which can pre-dissociate, breakdown of the molecular bond occurs. These two mechanisms are usually denoted as direct and indirect dissociation. Dissociative recombination cross section data have been produced for many molecules of atmospheric interest [173, 174, 175]. Among the vast literature a wide and up-to-date overview on dissociative recombination process can be found in [176].

## 3. Heavy particle collisions

### 3.1. Collision dynamics simulations

The calculation of molecular collisions observables, such as energy transfer cross sections and rate coefficients for gas phase systems is highly demanding already for masses, energies, temperatures and complexity of the interaction typical of the moderately large systems involved in the simulations. When more than three atoms are involved in a collision, it is impractical (and so far has not been attempted) to ground realistic simulations and related systematic computations on full dimensional quantum treatments integrating the associated scattering Schrödinger equations [177]. Because of this, related computations are usually carried out running QCT programs [178] or, sometimes, by combining quantum mechanics treatments (for selected bound degrees of freedom) with classical mechanics ones (for the remainder) within the so called quantum-classical method [179]. Seldom, and almost exclusively for three atom systems, the calculation is performed using exact quantum full dimensional treatments [180].

Recently, a computation scheme has been implemented, using a distributed workflow in a Grid Empowered Molecular Simulator (GEMS) [181], that considers in a sequence the *ab initio* calculation of the electronic structure of the molecular system,

its functional representation as an analytic PES spanning the whole configuration space covered by considered process, the detailed evaluation of the StS dynamics of the system, the statistical combination of the resulting detailed quantities to assemble *ab initio* generated observables. Once the PES has been built and validated against accurate spectroscopic and scattering information (including possible iterations), calculations are run to get reliable estimates of the cross section and rate coefficient values to feed as input to realistic simulations under different conditions (including those for which experiments cannot be performed). To ensure statistical accuracy large batches of classical trajectories are run and from their outcomes StS transition probabilities as well as detailed cross sections and rate coefficients for large numbers of ro-vibrational states, over a wide range of energies and temperatures, are obtained [42, 43, 44]. In this respect, the use of QCT techniques on parallel and distributed computing infrastructures has been the winning move in recent times because of the perfect decoupling of individual trajectories (or of small batches of them). However, the reliability of the results depends on the suitability of the QCT method for describing the collision process and on the accuracy of the PES in modeling long- and short-range intermolecular forces.

### 3.2. Molecule-molecule collisions

#### 3.2.1. Potential energy surfaces for the energy transfer

Even if in principle the intermolecular potentials can be characterized in detail by molecular beam scattering experiments [182] and spectroscopic studies of van der Waals complexes [183], the inference from the measured data is a difficult inversion problem. An accurate PES can be obtained by an efficient GEMS procedure that adopts a parametric model potential and then varies tentatively the value of the parameters so as to obtain from the integration of the dynamical equations the best possible agreement with experimental results to reproduce the glory oscillations and the second virial coefficient for diatom-diatom systems [55]. Moreover, since vibrations and rotations distort the molecular geometry, affecting both polarizabilities and charge distributions, the intermolecular forces, related to such properties, are strongly dependent on the quantum states of the interacting monomers and so are the outcomes of collision events. A suitable intermolecular potential energy surface should, therefore, definitely return the variations of the interaction with the internal coordinates of the molecules. For this reason those dimer PESs made of frozen monomer interaction terms cannot be considered truly adequate for modeling the energy transfer in gas phase systems and full-dimensional PESs should be provided instead.

For the mentioned reasons  $V$ , the functional representation of the PES of the two colliding molecules, should contain both the inter-molecular component  $V_{inter}$  (representing the interaction of the two molecules depending, as shown below in Eq. (12), on the center-of-mass distance  $R$  between the two molecules and on the angles  $\Omega$  denoting the set of angles defining their mutual orientation) and the intra-molecular one  $V_{intra}$  (representing the potential energy function of the two isolated molecules at infinite separation depending on the vector  $\mathbf{q}$  defining the internal coordinates of the two molecules). Accordingly,  $V$  is formulated as a sum of these two contributions:

$$V = V_{intra}(\mathbf{q}) + V_{inter}(R, \Omega; \mathbf{q}). \quad (12)$$

Note that  $V_{inter}$  depends parametrically on the molecular geometry  $\mathbf{q}$  in order to

incorporate the effects of the rotovibrational motion on the intermolecular forces. The internal interaction energy  $V_{intra}$  is often replaced by an *ab initio* ground state potential, while  $V_{inter}$ , being the interaction component pivoting the energy transfer, has to be accurately determined in order to ensure the realism of the simulations and the accuracy of the energy transfer probabilities, cross sections and rates.

A general versatile formulation of the term  $V_{inter}$  of Eq. (12) consists of a sum of two effective interaction components, *i.e.*  $V_{vdW}$  and  $V_{elect}$ , representing the van der Waals (size repulsion plus dispersion attraction) and the electrostatic reactant interactions, respectively. These two terms vary strongly with  $R$  while weakly depending on  $\Omega$ .  $V_{elect}$  depends on the anisotropy of the charge distributions of the two molecules and tends to the permanent quadrupole-permanent quadrupole interaction at large distances. However, when the two molecules come into closer contact during the collision (as is the case of long lasting collisions) the interaction between atoms originally belonging to different molecules should be taken into more explicit account. This is usually done by formulating the van der Waals term as an Improved Lennard-Jones (ILJ) potential [184] adding further flexibility to the PES.

A more general approach, is to combine contributions from different arrangements of the system already in the fitting procedure. A great advantage of these so-called *local* methods is the fact that the fitting can be improved by simply adding more *ab initio* points from nearby. Moreover the points need not be located on a uniform grid. This is the case of the Moving Least Squares (MLS) techniques which mix together global and local (basis functions which are only used locally to the geometry of interest) features of the interaction [185, 186, 187, 188, 189]. The enforcement of the symmetry of the system on the formulation of the PES can also be adopted. In preliminary studies of the  $N_2 + N_2$  [55] and  $O_2 + N_2$  [190] energy transfer processes reference is made to ILJ basis functions.

### 3.2.2. Quasiclassical and Quantum-classical calculations

A multi-dimensional PES of the type of Eq. (12) for a four-atom colliding system can be used to run QCT simulation at a StS level of details, accounting for the quantization of reactants and products.

The initial vibrational states of the colliding molecules are explicitly selected [191, 192, 92, 193, 184], while the initial rotational states are assigned by sampling a Boltzmann distribution at a given rotational temperature  $T_{rot}$ . This means that cross sections and probabilities obtained from the trajectories are specific for vibrational states, but thermally averaged over rotations. Note that rotational averaging reduces the number of quantum labels that have to be taken into account and the computational load. For the selection of the trajectory initial velocities two main alternative exists: (i) velocities are selected to give a fixed collision energy  $E$ ; (ii) velocities are selected randomly from a Boltzmann distribution at temperature  $T$  (translational temperature). The second option gives directly a set of initial and final states whose processing results in thermal probabilities and rate coefficients, assuming translation and rotational degrees of freedom in equilibrium ( $T_{rot} = T$ ). The set of final product states have to be presented in a quantum fashion by a quantization procedure. The simplest representation of the vibrational energy of diatomic and triatomic molecules is obtained by approximating the vibrational motion as that of a set of independent harmonic oscillators. In this way the energies of each vibrational mode can be obtained by projecting the final phase space vectors of the products into the normal mode vectors. Accordingly, a data-binning can be performed to obtain

vibrational quantum numbers, by simply rounding the ratios of the energy content of each vibration mode to the corresponding energy spacing, to the closest integer. A slightly more accurate procedure relies on the Einstein-Brillouin-Kramer (EBK) quantization rule, based on the action integral, for each vibrational coordinate (e.g. a normal mode), over an entire period. After the action integrals, the obtained “non-integral” quantum numbers have to be binned.

As already anticipated, a more rigorous approach (and therefore a more significant validation test of the results obtained) has been taken for the  $N_2 + N_2$  [55] and  $O_2 + N_2$  [190] systems by employing quantum-classical treatments. The goal of such effort has been, on one hand to calculate an accurate sets of vibrationally selected rate constants for multi-quantum VV and VT exchanges in a broad range of gas temperature, and, on the other hand to evaluate the conditions in which the QCT treatment agrees better with quantum-like treatments. For the diatom-diatom systems considered, one can treat molecular vibrations quantum-mechanically by integrating the related time-dependent Schrödinger equations while treating classically rotation and translation by integrating the related Hamilton equations. The two subsystems, and the corresponding equations of motion, are dynamically coupled through the definition and calculation of a time-dependent “effective” Hamiltonian and the time evolution of the total wavefunction is obtained by expanding it over the manifold of the product, rotationally-distorted, Morse wave functions of the two isolated molecules. Then, the Hamilton equations for the ro-translational motions are integrated self-consistently together with the Schrödinger equations of motion of the vibrational amplitudes (the number of vibrational levels, above and below the initial vibrational state of the colliding diatoms included in the wave function expansion, depends on the initial vibrational state of both molecules and on the impact kinetic energy). From the square modulus of the amplitude of the vibrational transition the detailed quantum classical estimates of the cross section and rate coefficient can be worked out (by integrating over energy and averaging over the initial Boltzmann distribution of kinetic and rotational energies respectively) and compared with QCT ones.

The classical approximation for the rotational motion of the two colliding molecules imposes a lower limit to the gas temperature (around  $T = 200$  K for the  $N_2$ - $N_2$  and  $N_2$ - $O_2$  systems), moreover a quantum description of the molecular rotations have a slight impact on the rate constants at the lower temperature limit. Therefore, the quantum-classical method, also known as semiclassical coupled-state method according to the first formulation given by Billing [194] is quite accurate over a wide temperature range; this accuracy is mainly determined by the accuracy of the interaction potential. Extensive data base of state-selected rate constants [195, 54, 196] have been calculated within the quantum-classical approach for a number of diatom-diatom systems relevant to kinetics of laboratory low-temperature/low-pressure plasmas and in aerothermodynamics. It is worth noting that the semiclassical rate constants are, quite often, taken as reference rates to check the accuracy of analytical rate constants based on first-order dynamical approximations [56]. Figure 11 compares the QCT and semiclassical methods for a set of StS rate coefficients for the  $N_2+N_2$  system (for details see Ref. [55]). One can see that semiclassical rates are in general smaller than the QCT ones (although still of the same order of magnitude) except for the quasi-resonant transition (25;25|24;26), a case in which semiclassical values are, on the average, 20 % smaller. Results for the  $N_2+O_2$  system are shown in Figure 12, reporting a comparison of experimental and semiclassical rate coefficients for the  $O_2(v_a) + N_2(v_b = 0) \rightarrow O_2(v_a-2) + N_2(v_b = 1)$  vibrational transitions, with  $v_a$ ,

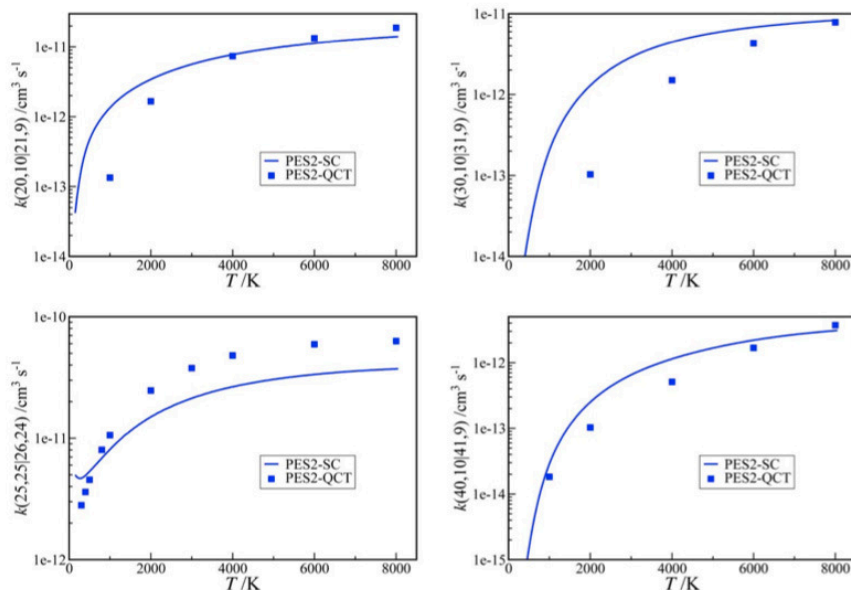


Figure 11: QCT (markers) and semiclassical (solid lines) rate coefficients [55] as a function of temperature for the transitions:  $\text{N}_2(v_a) + \text{N}_2(v_b) \rightarrow \text{N}_2(v_a + 1) + \text{N}_2(v_b - 1)$ . Upper-left panel:  $(v_a = 20, v_b = 10)$ ; upper-right panel:  $(v_a = 30, v_b = 10)$ ; lower left panel: quasiresonant  $(v_a = 25, v_b = 25)$ ; lower right panel:  $(v_a = 40, v_b = 10)$ .

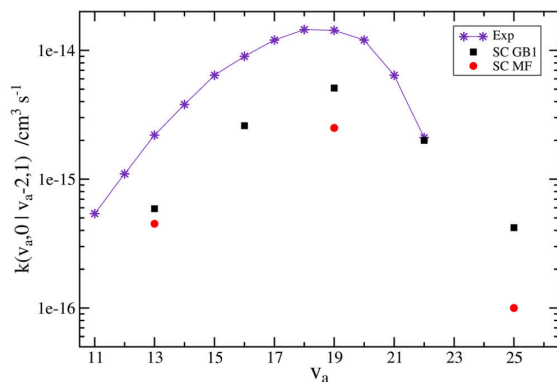


Figure 12: The  $\text{O}_2(v_a) + \text{N}_2(v_b = 0) \rightarrow \text{O}_2(v_a - 2) + \text{N}_2(v_b = 1)$  semiclassical rate coefficients at  $T = 300$  K calculated and compared with experimental results of Ref. [197].

the nitrogen vibrational quantum number, varying from 11 to 25. The rate coefficients are calculated using two different  $\text{N}_2\text{-O}_2$  intermolecular PESs, denoted as GB1 [198] and MF [190]. For the  $\text{N}_2\text{-O}_2$  system, a comparison of the semiclassical and QCT methods is provided in Figure 13, where are shown the rate coefficients at  $T = 1000$  K calculated on the two PESs, GB1 and MF, for single and double quantum vibrational de-excitation of the process  $\text{O}_2(v_a) + \text{N}_2(v_b = 0) \rightarrow \text{O}_2(v'_a) + \text{N}_2(v'_b = 0)$ . It can be

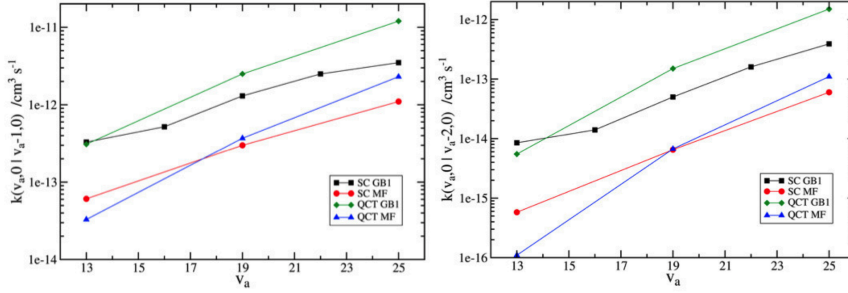


Figure 13: SC and QCT rate coefficients at  $T = 1000$  K calculated on GB1 [198] and MF [190] for single (left panel) and double (right panel) quantum vibrational de-excitation of the process  $\text{O}_2(v_a) + \text{N}_2(v_b=0) \rightarrow \text{O}_2(v'_a) + \text{N}_2(v'_b=0)$ .

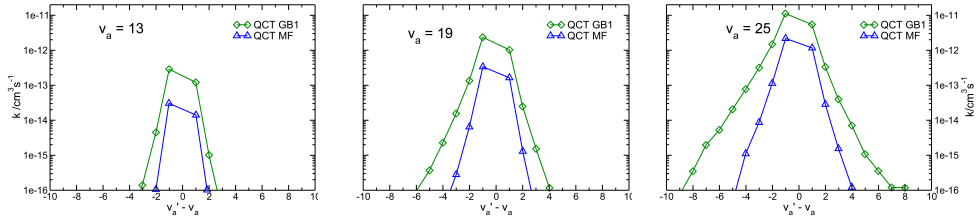


Figure 14: QCT rate coefficients at  $T = 1000$  K calculated on GB1 [198] and MF [190] PESs for multi-quantum vibrational excitation and de-excitation of the process  $\text{O}_2(v_a) + \text{N}_2(v_b = 0) \rightarrow \text{O}_2(v'_a) + \text{N}_2(v'_b = 0)$ .

seen that QCT results reproduce reasonably well the behavior of the semiclassical rate coefficients. Rate coefficients of multi-quantum transitions of type  $\text{O}_2(v_a) + \text{N}_2(v_b = 0) \rightarrow \text{O}_2(v'_a) + \text{N}_2(v'_b = 0)$ , for different initial values of the  $\text{O}_2$  quantum number  $v_a = 13, 19$  and  $25$ , and as obtained from the two potential energy surfaces GB1 and MF, are shown in Figure 14.

### 3.3. Atom-molecule collisions

Collisions of atoms with diatomic molecules are nowadays commonly treated with approximate or “exact” quantum mechanical (QM) methods [199, 200] or semiclassical approximations [201]. However, when dealing with the application into detailed models, normally reactive and non-reactive processes as well as dissociation/recombination have to be considered from and to the whole sets of molecular rovibrational states for both reactants and products, possibly on more than one PES, in quite large collision energy ranges. In this context it is obvious to use more approximate methods, such as Schwartz-Slawsky-Herzfeld (SSH) theory [202, 52, 203], forced harmonic oscillator [204, 205], and QCT, in order to use reasonable amounts of computational resources. QM methods can be used to assess the validity of a limited number of transitions treated with more approximate methods. However, it is important to realize that the reliability of a QM result is strongly dependent on the specific conditions and approximations in which the calculations are carried

out. Even treating all degrees of freedom of the system quantum mechanically (these calculations are generally intended as “accurate”), it is common to calculate the dynamics only for the first or very few values of total angular momentum  $J$ , using various approximations to obtain the cross sections or rate coefficients, because of the need of keeping low the computational load required, which increases very rapidly with  $J$ . These approximations are accurate for very low collisional energy values, but when more than thermal energies are considered, as those needed for example in aerothermodynamics, their reliability must be carefully assessed. For approximations which reduce the number of degrees of freedom, such as the infinite-order-sudden approximation (IOSA [206]), which neglects in particular molecular rotation, it is very difficult to estimate their reliability without comparisons with accurate calculations. The role of molecular rotation is nowadays largely acknowledged in aerothermodynamics [23]. Even if only a vibrational kinetics is often considered in most calculations, initial rotation should be at least considered as a parameter. However, if dissociation/recombination is important in a given kinetic scheme (and it is very likely that it is important for sufficiently high energy), then rotation should be explicitly considered [64]. Conversely, quasiclassical calculations tend to be more and more reliable for increasing total energy values. This means that rotational effects and dissociation can be obtained with a high level of accuracy for sufficiently high energy values. A particularly striking comparison of different quantum mechanical approximations with respect to quasiclassical results for reaction in a very light atom-molecule collisional system is presented in Ref. [207]. In that paper, different QM approaches (time independent, wave packet and approximate ones) are compared with quasiclassical results using the same PES. While for collisional energy less than 70 meV the agreement is good only among QM methods (including the approximate one, but only for energies lower than 20 meV), for energy values between 0.1 and 1 eV the agreement between QCT and time independent QM is undoubtedly the best one. In the same interval wave packet calculations show a significant discrepancy, while the approximate QM appears as unreliable. This is another strong confirmation that QCT can be considered the method of choice for heavy particle collision applications when sufficiently high temperatures are considered, as in aerothermodynamics.

### 3.3.1. $N+N_2$

One of the most important collisional systems to consider for the modeling of aerothermodynamics is  $N+N_2$ , on which topic there is a significant literature nowadays. The first PES historically available for this system was the semiempirical LEPS PES of Laganà and Garcia [208, 209]. These authors have also calculated many vibrational transitions by means of QCT, and their results have been used in models [210, 211], after some interpolations. It is important to emphasize that in order to use data in detailed kinetic models it is necessary to have the complete network of possible transitions among the whole rovibrational ladder of initial and final molecules, or at least a good guess for neglecting some specific transitions. Interpolations and extrapolations to obtain missing data from an incomplete set of transitions can cause large errors in the simulations [212]. This is the reason for calculating as complete as possible set of transition rates among the initial and final rovibrational states. However, in the  $N+N_2$  case one should consider almost 10000 rovibrational states, so some strategy is needed for minimizing the computational effort. In [213, 214] the strategy consists of limiting the number of initial vibrational states (one in five), considering some values of rotational temperature (allowing

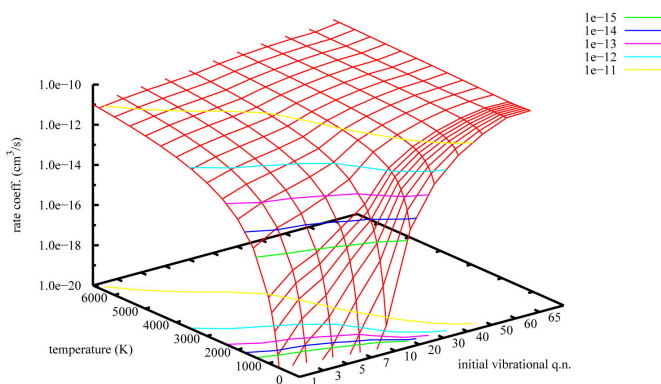


Figure 15: Monoquantum vibrational de-excitation rate coefficients for  $N+N_2$  ( $v, T_{transl} = T_{rot}$ ) as a function of initial vibrational quantum number and ro-translational temperature [215].

rotation to be considered as a parameter in simulations). In [42] all the reactants' rotational states are considered, but only about one in ten initial vibrational states. A graphical representation of the monoquantum de-excitation rate coefficients obtained in [215] is given in Figure 15, where the rate coefficients are shown as a function of initial vibrational quantum number and ro-translational temperature. It is clear that in this case the trend is quite smooth, without special issues concerning the interpolation. In fact rate coefficients can be interpolated on initial vibration with fairly good results, as in [42], but if cross sections are needed in the simulation, as in a Direct Monte Carlo approach [216], their interpolation is much more difficult and uncertain, with large possible errors.

In [217] all the initial vibrational states are considered, but initial rotation is limited to some values. However, using data without an interpolation on rotation can cause inaccuracies. Probably the best strategy is to use a simple linear interpolation between increasing non-contiguous values of initial rotation. This approach has been tested for similar systems [94] with good results. In [49] the whole ladder of rovibrational states have been considered in calculations, using a mixed approach including both some points on the energy axis for low collisional energies and some translational temperatures to distribute other points, in order to keep the computational load to a feasible level. In the cited work a very accurate *ab-initio* PES has been used [199], having a metastable  $N_3$  state in the strong coupling region (the so-called “Lake Eyring” feature [199]). This feature has subsequently been reproduced also in other studies of the same system [218, 219]. Some preliminary comparisons between VT data obtained in [218] and in [215] including just  $v = 0, 1$  initial vibrational states show that for reactive processes a discrepancy is seen and is justified by the absence of the Lake Eyring as well as by the significantly lower reaction barrier in the LEPS PES. Nevertheless, non-reactive rate coefficients appear quite similar. A detailed study (including higher vibrational states as well as dissociation) is needed to appreciate the differences between the two PESs, that cannot be expected to be completely negligible. A complete public dataset of cross sections on this accurate PES does not exist, and it is not simple to obtain, because of the high computational cost of the numerical calculation. It is important to understand that

from a computational point of view there are huge differences among different PESs of the same system, both for purely computational problems (sometimes the numerical code of the PES is not amenable to be easily rewritten for better performance) and for an intrinsic complexity of the dynamics involved (as in the case of the presence of the Lake Eyring, where the collisional system can spend a lot of time). This has the consequence of producing datasets of cross sections which are not optimal for modeling, because of large statistical errors due the reduced set of trajectories used in order to keep the computational load to an affordable level. Computational performance in calculation of large sets of dynamical data is fundamental, and it strictly depends on the performance of the PES. This point can appear as secondary when obtaining a new PES fit, with the greatest attention devoted to accuracy, but from the point of view of applications it should be carefully considered.

*3.3.2. O+O<sub>2</sub>* This collisional system is particularly interesting from a dynamical point of view, because of the possible formation of O<sub>3</sub> as a transient species during the scattering process. From a computational as well as a modeling point of view, on the contrary, this results in a triple drawback: the PES is quite difficult to obtain, the dynamics is generally very complicated and long [220], and simple models for data can hardly substitute true dynamical calculations. Moreover, this system has also excited electronic states lying no more than about 1.2 eV from the ground state, casting doubts on the reliability of purely adiabatic dynamics in the hyperthermal regime. In recent years many studies have been conducted on this system including excited electronic states, but in very few cases the PESs are actually available for calculations. It should be considered that there are also significative variations among PESs of different authors, as in the case of negative or positive temperature dependence of reactive rate coefficient around room temperature, as a consequence of the absence or presence of a tiny barrier (a “reef” structure) in the entrance and exit channels [221]. Better agreement with experiments would require a negative dependence, as found by Varandas and Pais [222] and more recently by [221] (see also dynamical results in [223]). From the point of view of modeling for aerothermodynamics, however, available data are from [47], with a limited treatment of initial vibrational states, and from [220, 223], where both dissociation and vibration-translation (VT) rate coefficients are present from many initial vibrational states and a complete treatment of molecular rotation on the [222] PES. Suited rate coefficient interpolations in [224] give a complete treatment of the full vibrational ladder. The results are freely available in [19], with good global comparisons with experimental data. A graphical representation of available rate coefficients for vibrational mono-quantum de-excitation [220, 223] is in Figure 16, with similar conditions to those in Figure 15. From the comparison of the two figures, it is clear that the trend is completely different. The range of rate-coefficient values is less than one order of magnitude for oxygen, while in the nitrogen case with the LEPS PES it is of many orders of magnitude. This striking difference is due to the presence of the metastable O<sub>3</sub> in the PES, which acts as a redistributor of vibrational energy among initial and final vibrational states. In [7] comparisons of reactive and non-reactive VT rate coefficients are shown for H+H<sub>2</sub>, N+N<sub>2</sub> with a PES without the “Lake Eyring” feature and O+O<sub>2</sub>. In this last case the absence of a barrier on the Varandas and Pais PES allows quite similar behavior for both reactive and non-reactive processes, with the only difference of a clear elastic peak as a function of final vibrational state for any given initial vibrational state. Apart from this peak, the trend is almost flat for de-excitation, because of the statistical equipartition of vibrational

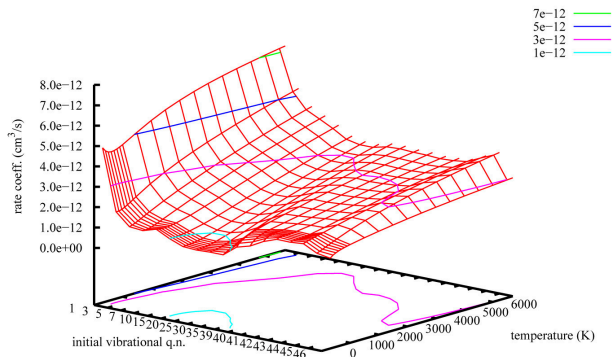


Figure 16: Monoquantum vibrational de-excitation rate coefficients for  $O+O_2$  ( $v, T_{transl} = T_{rot}$ ) as a function of initial vibrational quantum number and rotational temperature [220, 223].

energy due to the presence of the  $O_3$  well, as in the preceding discussion for  $N_3$  with Lake Eyring. While the elastic peak with quasi-elastic shoulders typical of the non-reactive part can be correctly described by simple methods based on quantum-classical correspondence of a forced harmonic oscillator, the flat trend common to reactive and non-reactive processes of this system can hardly be reproduced by these methods.

### 3.3.3. $O+N_2$

This is another very interesting collisional system for which few detailed calculations are present in literature. The reaction to form NO is endothermic by more than 3 eV, so calculations have been generally performed in the opposite direction to benefit from higher probabilities. One notable exception is [44], where quasiclassical and wave packet calculations are compared with good results for sufficiently high total energy, as expected. The features of the two accurate uncoupled triplet PESs used are dynamically studied, with interesting effects due to the presence of metastable states in the strong coupling region (SCR). These effects can also be stressed by comparing different collisional systems from a given initial vibrational state,  $v = 40$  in Figure 17, where the vibrational energy exchange rate coefficient is shown as a function of final vibrational quantum number for  $O+N_2$ ,  $N+N_2$  and  $O+O_2$ , in the non-reactive case. While for  $N+N_2$  the LEPS PES is adopted (without any metastable state), in the other two cases the presence of a minimum in the SCR deeply affects the final vibrational distribution of probabilities, with a clear tendency to a flat trend (except the elastic peak and its shoulders). A more complete work on this system is in preparation by some of the present authors, with very detailed database of both VT and dissociation. Some preliminary results have been presented in [94]. The non-reactive process, however, shows important issues. The comparison with experimental data is acceptable only for temperatures higher than 4000 K, while twenty orders of magnitude of discrepancy can be found at room temperature. It is very likely that for intermediate regimes of temperature it is necessary to investigate to what extent this issue can affect aerothermodynamical models. However, this investigation is not free from serious difficulties. In [225] it is shown that, while quasiclassical trajectories are unable to reveal any inelastic transition at room temperature (it is a “classically forbidden” process [226]), a quantum approximate calculation is able to give a non-

zero rate coefficient, but too low to be in quantitative agreement with experimental values. As also suggested from those authors, a more accurate study should include a nonadiabatic spin-forbidden transition from the triplet surfaces correlating with  $O+N_2$  in their respective ground states to the singlet PES of  $N_2O$ . The formation of a long

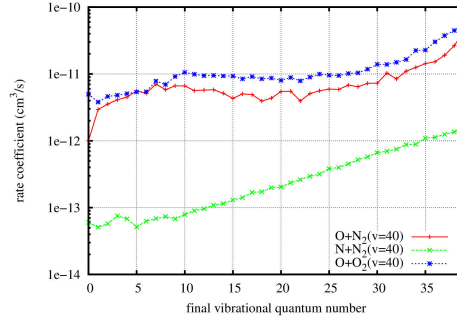


Figure 17: Comparison of vibrational de-excitation rate coefficients for the collisional systems  $O+N_2$ ,  $N+N_2$  and  $O+O_2$  from the initial vibrational quantum number  $v = 40$  ad for  $T = T_{rot} = 300$  K.

lasting complex on this surface with final exit on the triplets could have the effect of a flat vibrational distribution in products, that could explain the large VT rate coefficients in the experiment. This investigation requires the singlet surface of  $N_2O$ , the couplings with the two triplets of  $O+N_2$ , and the treatment of non-adiabatic transitions both by a classical method as well as a semiclassical or approximate quantum method, in order to better understand the nature of the effect.

### 3.4. Atom-molecule collisions: applications

The availability of a very accurate and complete set of QCT StS rate coefficients, including dissociation rates, allows to obtain more precise results in many aerospace applications including the hypersonic boundary layer. In the past the Ladder Climbing (LC) dissociation model has been widely used [5, 227, 211, 68]. LC adds to the bound levels of the vibrational ladder a pseudo level located just above the last bound level *i.e.* in the continuum. In turn the dissociation rate is calculated by extrapolating the bound-bound VV and VT rates to the pseudo level. In a  $N_2/N$  mixture, the large differences between the results obtained by using QCT rates and ladder climbing (LC) ones are observed in the hypersonic boundary layer flows as well as in nozzle expanding flows [27, 228]. In the following only results obtained with the QCT model (Figure 18 and Figure 19) will be reported. In the boundary layer flow the gas temperature strongly decreases from the edge of the boundary layer ( $\eta = 8$ ) to the surface ( $\eta = 0$ ) (Figure 18a) promoting the corresponding dissociation-recombination kinetics and creating non-Boltzmann vibrational distributions (Figure 18b). In this figure we can observe plateau in the vibrational distribution at different distances from the surface  $\eta$  resulting from the preferential pumping of vibrational levels by the recombination process. These non-equilibrium vibrational distributions generate an anti-Arrhenius behavior of the dissociation constant versus  $\eta$  in the region  $0 < \eta < 2.5$  (Figure 18c) *i.e.* the dissociation constant increases decreasing the gas temperature.

Similar results have been obtained for the  $N_2/N/O_2/O/NO$  mixture where the

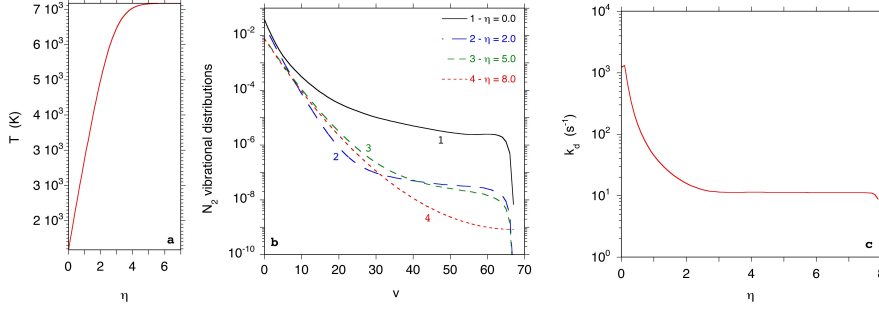


Figure 18: (a) Gas temperature  $T$  along the normal to the body surface,  $\eta$ , in the hypersonic boundary layer under study, (b) nitrogen vibrational distributions at different distances from the surface and (c) pseudo-first-order dissociation constants as a function of  $\eta$ , calculated according to the QCT model. The mixture is a  $N_2/N$  one with wall temperature  $T_w = 1000$  K, edge temperature  $T_e = 7000$  K, pressure  $P_e = 1000$  N/m $^2$ , inverse of the residence time in the boundary layer  $\beta = 5000$  s $^{-1}$  [27].

different QCT rates reported in this review have been used [26]. In addition results for the  $CO_2/CO/C/O_2/O$  mixture relevant to Mars entry aerothermodynamics can be found in Refs. [88, 70, 229].

Another case study deals with non-equilibrium in boundary layer kinetics of an  $O_2/O$  mixture [28] for partially catalytic and no-catalytic surfaces. In the case of partially catalytic surface the molecular dynamics results presented in Section 4, where it is shown the preferential pumping of vibrational levels during the heterogeneous recombination, were used. In Figure 19 the pseudo first order dissociation rate as

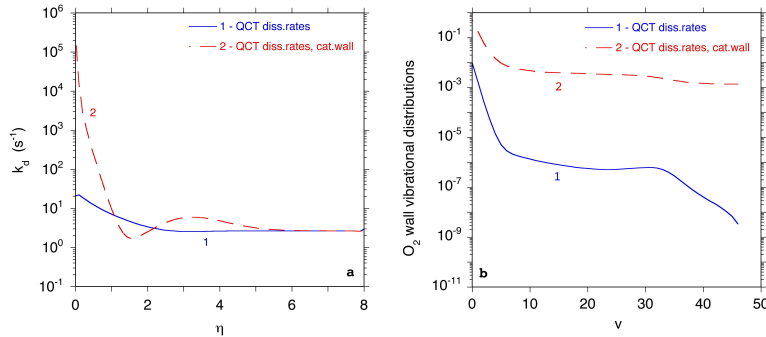


Figure 19: (a) Pseudo-first-order dissociation constants as a function of  $\eta$  in the hypersonic boundary layer under study and (b) wall oxygen vibrational distributions calculated according to the QCT model both in the case of a no catalytic surface and in the case of a partially catalytic one. The mixture is a  $O_2/O$  one with  $T_w = 1000$  K,  $T_e = 4000$  K,  $P_e = 1000$  N/m $^2$ ,  $\beta = 5000$  s $^{-1}$ . The heterogeneous recombination coefficients are from reference [69].

a function of  $\eta$  (Figure 19a) and the vibrational distributions close to the surface (Figure 19b), obtained considering either a no-catalytic surface or a partially catalytic one [69] are reported. The results emphasize the importance of using molecular

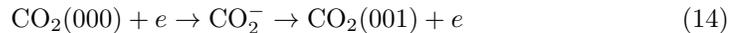
dynamics methods either for the gas phase or for the gas surface interaction.

### 3.5. The prototypical case of CO<sub>2</sub> plasmas

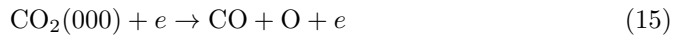
Large theoretical and experimental interest is presently dedicated to the activation, *i.e.* dissociation, of CO<sub>2</sub> under cold plasmas as well as in aerospace technology (Mars entry problems as well propellant in helicon electrical thrusters). In both cases the dissociation process stimulated by vibrational excitation plays an important role implying a strong effort in the corresponding theoretical characterization. Pure vibrational mechanisms against mechanisms induced by direct electron impact have been recently reconsidered in the case of N<sub>2</sub> and CO plasmas [24]. In this session we want discuss the same mechanisms for CO<sub>2</sub> molecules stressing the most important cross sections acting in the system. In CO<sub>2</sub> plasmas, especially at low electron temperature ( $T_e \leq 2$  eV), the input of electrical energy goes through the excitation of vibrational modes of CO<sub>2</sub> (in particular the asymmetric one) followed by VV energy exchange processes able to spread the low-lying vibrational quanta over the whole vibrational ladder of CO<sub>2</sub>, ending in the dissociation process. The upper limit to the pure vibrational mechanism can be obtained by the simplifying Eq. (13) [24]

$$K_d^{ulPVM} = \frac{1}{v_{max}} k_{eV}(0 \rightarrow 1) \quad (13)$$

where  $k_{eV}(0 \rightarrow 1)$  is the rate of the resonant (000)  $\rightarrow$  (001) vibrational excitation process and  $v_{max}$  the number of vibrational quanta contained in the vibrational ladder of CO<sub>2</sub>. Eq. (13) assumes that the vibrational quanta on the asymmetric vibrational ladder of CO<sub>2</sub> introduced by electron-molecule resonant processes are transported by a VV up pumping mechanism to the dissociation continuum. This rate can be several orders of magnitude higher than the corresponding dissociation process induced by electron impact from the ground state [95]. The calculation of Eq. (13) requires the knowledge of the cross sections for the resonant vibrational excitation process



as well as a Boltzmann solver to get the electron energy distribution function (eedf) of the cold plasma. The Boltzmann solver should contain elastic, inelastic, dissociation, ionization and superelastic cross sections of the CO<sub>2</sub>. One of the most used data bases for CO<sub>2</sub> is that one compiled by Phelps [230, 231] referring to the interaction of electrons with CO<sub>2</sub>(000). In particular the Phelps database contains eV transitions over the other vibrational modes of CO<sub>2</sub> including some combined levels. Use of the Boltzmann solver with the reported cross sections allows us to calculate  $K_d^{ulPVM}$  and to compare it with the corresponding direct dissociation rate  $K_d(v = 000)$ , *i.e.* of the process



The comparison as a function of  $E/N$  in the presence or absence of superelastic vibrational collisions confirms, at least for  $E/N < 50$  Td, the old hypothesis, *i.e.*  $K_d^{ulPVM} > K_d(v = 000)$ [95]. The accuracy of the different rates can be hopefully estimated to one or two orders of magnitude, this (in)accuracy reflecting on the incomplete sets of electron molecule cross sections and influencing the eedf (and in turn the rates of electron-impact induced processes). To understand this point in Refs. [95, 232] has been recalculated the hierarchy of the different rates by introducing in

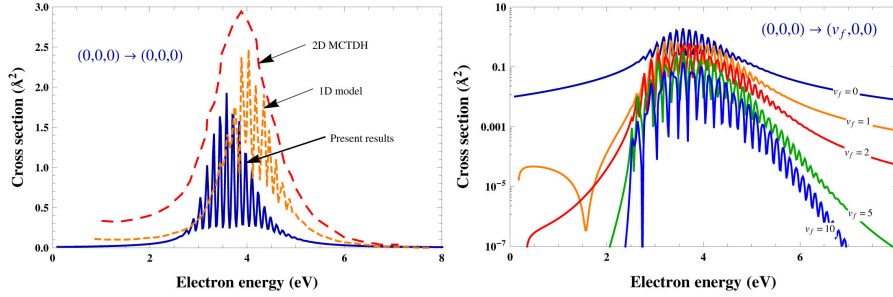
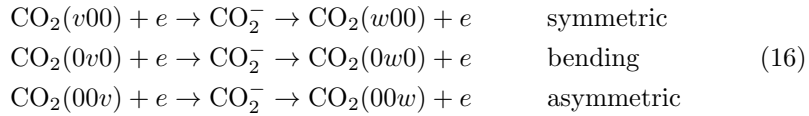


Figure 20: (left) Elastic electron- $\text{CO}_2$  resonant cross section: 1D results of Laporta et al [91] (solid line) compared with 1D boomerang model (short-dashed line) and MCTDH (the long-dashed) from Ref. [234]; (right) electron-impact resonant excitation of  $\text{CO}_2$  symmetric modes,  $(0,0,0) \rightarrow (v_f,0,0)$ , for different values of the final symmetric vibrational quantum number [91].

the Boltzmann solver all eV cross sections linking the asymmetric ladder, calculated by using the scaling law of Fridman [233]. The results show that this addition of cross sections, while not affecting the hierarchy of rates, strongly affects the absolute values of electron impact dissociation rates through changes in eedf. A similar strong influence should be expected if one introduces in the Boltzmann solver all eV transitions including the different modes of  $\text{CO}_2$ , *i.e.* the processes:



An attempt in this direction has been done by Laporta et al [91] by considering the independent vibrational modes of  $\text{CO}_2$ . The resonant cross sections and the corresponding rate coefficients for electron- $\text{CO}_2$  scattering were studied in the framework of  $R$ -matrix method [155], by considering the separation of the modes approximation. The potential energy surface of the ground electronic state of  $\text{CO}_2$  was obtained by MOLPRO [166] an *ab initio* quantum-chemistry package. In both calculations the cc-pvQZ basis and the MRCI model was used. Some cross section results are shown in Figure 20.

Coming back to Eq. (13), we must emphasize that this equation gives only the maximum contribution of a pure vibrational mechanism in the absence of any VV and VT energy transfer processes. The situation may be largely improved by solving an appropriate vibrational master equation of the three modes of  $\text{CO}_2$  [235, 236, 88]. A lot of problems arise in this description, the most important of them being the calculation of complete data set for VV and VT processes occurring in the system. Complete sets of VV and VT rates can be calculated by the SSH theory scaling through corresponding theoretical values over the lower vibrational levels. More recently Lombardi et al have obtained a set of VV and VT rates by running QCT on an accurate PES. The master equation used by Armenise and Kustova [88] covers conditions where vibrational excitation affects the dissociation recombination regime in hypersonic flows without considering the presence of electrons. Neglecting the electron-molecule collisions is the weak point of this model that should be overcome. Unfortunately insertion of this accurate model in non equilibrium plasma kinetics

scheme is sometimes prohibitive for the number of excited levels. In this sense the vibrational master equation developed by Bogaerts et al [236], describing the asymmetric mode linked to the other modes by some intermode VV and VT energy transfer reactions, is an attempt to investigate the vibrational state of the CO<sub>2</sub> molecule with a reduced vibrational model. Again the set of VV and VT rates are scaled by using the SSH theory and some experimental and theoretical values of the low lying vibrational levels. The accuracy of these rates can be again checked against the QCT estimates of Lombardi. In the Bogaerts et al [236] vibrational kinetics an effort is also made on the role of vibrational excitation in affecting the dissociation rates of CO<sub>2</sub> by heavy particle collisions. They use a kinetic approach essentially based on the absolute theory of chemical reactions where vibrational excitation decreases the activation energy of the process. Of course, QCT calculations can be a further improvement in the process provided the PES used for VV and VT rates by Lombardi et al. and allow to add reactive channels and further check by comparison with quantum classical results.

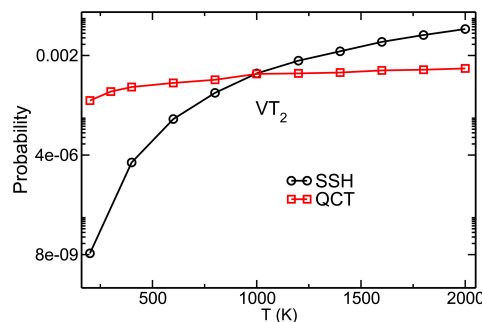


Figure 21: The  $VT_2$  probabilities are shown as a function of temperature and compared with the corresponding results from SSH theory [235].

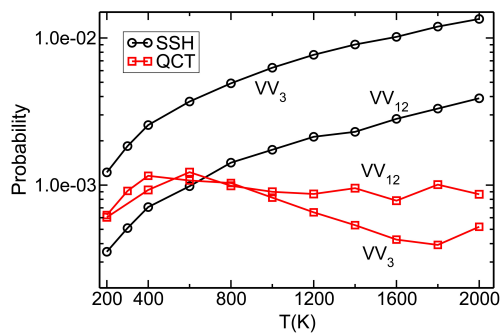
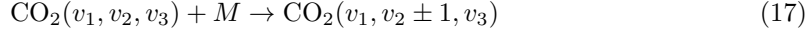


Figure 22: The  $VV_{12}$  and  $VV_3$  probabilities, as a function of temperature, obtained from QCTs are compared with the corresponding results from SSH theory [235].

Energy exchange probabilities obtained by QCT are shown in Figures 21 and 22 for VV and VT processes as a function of the temperature  $T$  and compared with the corresponding values from the SSH theory from Ref. [235]. Figure 21 shows the probability of  $VT_2$  energy exchange (vibration-translation exchange involving a quantum of bending vibrational energy). According to the classification provided in Ref. [235],  $VT_2$  processes are as follows:



where  $v_2$  is the quantum number of the doubly degenerate bending mode of  $\text{CO}_2$ . Figure 22 the QCT energy transfer probabilities as a function of the temperature  $T$  for  $VV_3$  and  $VV_{12}$  vibration-vibration exchange processes, where, according to the classification proposed in Ref. [235], a quantum of energy of asymmetric stretching goes from one to another of the colliding  $\text{CO}_2$  molecules ( $VV_3$ ) and a quantum of energy of the symmetric stretching goes into the bending mode ( $VV_{12}$ , intramolecular energy transfer). To obtain the  $VT_2$  and  $VV_3$  thermal probabilities, a batch of  $\sim 7$  millions of trajectories has been run, with initial vibrational state  $(0, 0, 1) + (0, 0, 0)$  and temperatures ranging from 200 to 2000 K. The choice of such an initial vibrational state of the molecules permits one to directly calculate  $VV_3$  rates (here presented as probabilities, to be compared with SSH results) and to give an estimation of the  $VT_2$  rates, measuring the probability of the transfer of energy from translations to the bending mode of  $\text{CO}_2$ . A different smaller set of trajectories, with initial vibrational states  $(n, 0, 0) + (0, 0, 0)$ ,  $n = 1, \dots, 5$ , has been used to obtain an estimation of the  $VV_{12}$  processes probability in the given temperature range. Marked differences can be seen to exist between QCT and SSH probabilities, especially for the  $VV_{12}$  and  $VV_3$  processes at temperatures higher than 800 K. This can be in part due to the sensitivity of the QCT StS results to the initial vibrational states. However, the deep causes of such disagreement can be numerous, and have to be searched in the approximations underlying the SSH theory, which may compromise the capability of the theory of furnishing correct results, or, on the other hand, in some degree of arbitrariness always present in the procedure adopted to quantize the classical final vibrational states in the QCT method. Experimental data, mostly lacking, would be extremely useful for validation.

#### 4. Gas-surface processes

The catalytic properties of surfaces can be studied in a very detailed way by the MD simulations that enable to describe at atomic level the elementary processes due to the interaction of gaseous species (atomic or molecular) with solid surfaces. These processes include atomic and molecular adsorption (sticking), elastic and inelastic scattering, recombination (ER, LH and HA) and molecular dissociation. In particular, recombination process is an effective source of ro-vibrationally excited molecules and, at the same time, is effective for surface atom abstraction and atom/molecule removal from the plasma region [67]. Moreover, adsorbed species, the initially adsorbed species or the new-formed molecules, will desorb. On the other hand, two additional homogeneous processes, diffusion of reactants on to the surface and diffusion of products away from the surface will also happen. ER and LH processes will compete depending on the experimental conditions. Commonly LH mechanism will be more favourable at low temperatures due to the high surface coverage. At higher

temperatures, with a much lower coverage, ER and HA mechanisms will become more important, unless the mobility of adsorbed species is high.

Adsorption processes and recombination reactions will be exothermic processes more important than the endothermic desorption processes, hence producing an overall heat release to the surface. This heat flux is additional to molecular conduction and can achieve up to 40% of the total heat flux inside the stagnation region. Thus, TPSs should be poor catalytic materials (e.g. silica-based materials) and characterized by high emissivity and low thermal conductivity. In contrast, ablative TPSs can accommodate high heat fluxes through phase change and mass loss [237, 238, 239].

The exothermicity partitioning process is controlled by several molecular and surface parameters, as, in particular, the collisional mechanism that is behind the recombination reaction, the active surface sites involved in the interaction and, therefore, the nature, coverage and temperature of the substrate, the dynamical coupling between atoms/molecules and the surface. The number and complexity of these effects is evidently high. Indeed, this issue, *i.e.* the energy sharing mechanism in chemical surface processes, is among the most complex and intriguing problems relevant to re-entry condition simulations. In fact predictions of the TPS catalytic response made in various space missions have failed also due to the insufficient knowledge of the exothermic processes that can be active at the shuttle walls.

The predictive character of advanced kinetic models of the boundary layer [69, 240] in estimating the heat flux to the TPS tiles relies on the knowledge of: 1) StS recombination probability,  $P_i(v|E_{kin})$ , *i.e.*, the probability that  $i$ -atom or molecule recombine at the surface forming a molecule in  $v$  vibrational level for a given collisional energy,  $E_{kin}$ ; 2) global and state-selected recombination coefficient,  $\gamma_i(T_S)$  and  $\gamma_i(v|T_S)$ , *i.e.* the fraction of total atoms (or molecules) in the incoming flux that ends in molecular form and in a given vibrational quantum number,  $v$ , after colliding for a given surface temperature,  $T_S$ ; 3) energy accommodation coefficient,  $\beta_i(T_S)$ , the ratio of energy released to the surface per atomic recombination to the maximum energy transferable; 4) the molecular vibrational distribution into the final states,  $N(v)$ , the probability that molecules form in a given vibrational quantum number; 5) state-selected dissociation probability,  $P(E_{kin}|\{.\}|v,j|T_S|)$ , the probability that molecule in  $(v, j)$  ro-vibrational levels, dissociates.

The lack of a collisional database of heterogeneous processes, except for the recent database Phys4Entry [19], is mainly due to the fact that surface processes are very specific. In fact, the sticking coefficient  $S$ , as well as the recombination coefficient  $\gamma_i$  depend upon some molecular behavior, such as the internal energy state, impact energy, orientation angles etc., of the reactants, but also upon the chemical-physics properties of the surface: structural and chemical composition, corrugations, coverage, which are strictly correlated to the conditions of the plasma environment. The determination of these surface parameters in real systems under operative conditions is obviously not an easy task.

Several studies about elementary surface processes occurring in Earth, Jupiter and Mars atmospheres with two materials, silica ( $\beta$ -cristobalite and  $\beta$ -quartz) and graphite that can be used as material models of real TPSs have been performed by some of the present authors. These surfaces are exposed to molecular oxygen, hydrogen, nitrogen and CO<sub>2</sub> fluxes, for the interest that these molecules and their dissociation species have for entry in Earth, Jupiter and Mars atmospheres. In spite of the major abundance of N<sub>2</sub> molecules compared to O<sub>2</sub> molecules in air, the much lower O<sub>2</sub> dissociation energy favours the atomic oxygen formation during re-entry

conditions and hence the O adsorption and the subsequent atomic recombination will become the most important elementary processes in Earth atmosphere.

#### 4.1. Oxygen, nitrogen, hydrogen and carbon oxide

In the pioneering paper concerning the recombination of oxygen atoms on a silica  $\beta$ -cristobalite surface [76], a switching of the reaction mechanism from ER to LH with the surface temperature decrease was pointed out. This result was stated by comparing the recombination coefficient obtained from MD simulations at different  $T_S$  with the corresponding experimental data available for O atom recombination on silica or silica-like surfaces. In another study [75], oxygen atom recombination on  $\beta$ -quartz was studied showing that, despite the common tetrahedral structure, the different binding configuration of the  $\text{SiO}_4$  tetrahedra gives rise to a different catalytic activity of the two polymorphs. The paper gave also a validation of semiclassical collisional method [241, 242], used in MD simulations, because a good qualitative and quantitative agreement was obtained between the theoretical and the experimental recombination coefficients in a wide range of surface temperatures. Evidence was also given of the higher catalytic response of cristobalite with respect to the quartz surface toward the O atom recombination ( $\gamma_{\text{O}}(\beta\text{-cristobalite}) > \gamma_{\text{O}}(\beta\text{-quartz})$ ).

Some years later, another study of atomic gas oxygen colliding with a clean  $\beta$ -cristobalite surface [243] was carried out by using classical trajectories for normal and off-normal incidence, 0.1-1 eV collision energies and surface temperatures between 300 K and 1100 K. The large adsorption energy for O over top Si atoms seems to play a key role in the dynamics of the sticking process; this is mainly produced via the absorption/penetration of O into the  $\text{SiO}_2$  slab instead of a simple adsorption. To see the effect of oxygen coverage in the O sticking process, which also competes with the ER reaction to produce  $\text{O}_2$ , a similar DFT-based PES was developed for the O+O/ $\beta$ -cristobalite system [244, 72]. Classical trajectories were calculated for 0.01-4 eV collision energies, several incident angles and surface temperatures between 100 K and 1500 K, with an O-precovered  $\beta$ -cristobalite surface. Atomic sticking was also the principal process, while  $\text{O}_2$  formation with the molecule finally adsorbed over the surface was the second one. Atomic oxygen reflection and ER reaction (*i.e.*,  $\text{O}_{2\text{gas}}$  formation) were much less important although also significant. The new  $\text{O}_2$  molecules produced by the ER reaction at high temperatures become internally and translationally excited, while the slab becomes colder. In order to evaluate all competitive heterogeneous processes occurring for an O/ $\text{O}_2$  gas mixture reacting on a silica surface, with different contributions into the global heat released to the surface, a microkinetic model was developed [73] for this system including 10 surface elementary reactions, among them the ER and LH processes. This study allowed to determine the atomic recombination coefficient  $\gamma_i$  and the chemical energy accommodation coefficient  $\beta_i$ . In this study, thermal rate constants were derived from previous QCT data of the forward processes or using the principle of detailed balance for reverse ones, in a wide range of temperatures (700 K - 1700 K). The computed  $\gamma_{\text{O}}$  mainly had contributions of the atomic sticking and ER recombination, being very small ( $0.01 < \gamma_{\text{O}} < 0.02$ ) and increasing with temperature, following an Arrhenius equation in agreement with experimental data (Figure 23). In the same temperature range, an estimation of  $\beta_{\text{O}}$  was obtained, the main contribution arising from the atomic sticking process instead of the ER or LH processes, with an almost constant value ( $0.75 < \beta_{\text{O}} < 0.80$ ), but different from the unity value assumed in earlier studies.

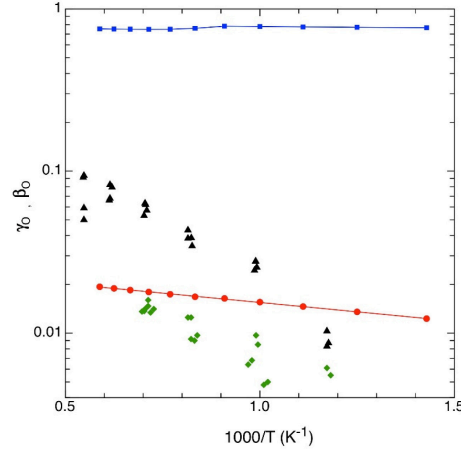


Figure 23: Calculated  $\gamma_{\text{O}}(T)$  (red circles with a least squares fitting line) and  $\beta_{\text{O}}(T)$  (blue squares with a simple line joining the points) coefficients versus the reciprocal of the temperature for an  $\text{O}/\text{O}_2$  reactant mixture ( $P_{\text{O}} = 91 \text{ Pa}$ ,  $P_{\text{O}_2} = 9 \text{ Pa}$ ) on  $\beta$ -cristobalite [73]. Some experimental values for  $\gamma_{\text{O}}(T)$  in air on  $\beta$ -cristobalite (black triangles) and quartz (green diamonds) at  $200 \text{ Pa}$  [245] are presented to be compared with.

Using a cluster approach, the interaction potential of atomic and molecular oxygen on  $\beta$ -cristobalite and  $\beta$ -quartz was determined *via* density functional theory (DFT) calculations in [78, 79], where the oxygen adsorption dynamics on  $\beta$ -cristobalite and  $\beta$ -quartz were studied. It turns out that the binding energy for the gas-phase O atom interacting on Si atom on the surface is almost the same for the two silica polymorphs, about 5.6 eV. On the contrary, interaction potential of a gas-phase oxygen interacting with the silica oxygen below the topmost Si atom layer is considerably different for the two silica polymorphs, being around 2.0 eV and 1.0 eV for cristobalite and quartz, respectively. The obtained PES was inserted in the semiclassical model [241, 242] to study the adsorption dynamics for oxygen atom on the two silica surfaces. The adsorption and inelastic scattering probabilities and the energy transferred to the surface in these two processes were determined in a large collisional energy regime,  $0.05 \text{ eV} < E_{\text{kin}} < 0.8 \text{ eV}$ . It turns out that, the probability for atomic adsorption and inelastic scattering is almost the same for the two silica polymorphs, while the energy transferred to the surface in the adsorption processes, is considerably higher in the case of quartz. This last result would indicate that a surface thermal damage should be more effective in the  $\beta$ -quartz as a result of an efficient chemical conversion scheme that funnel the kinetic energy of the impinging oxygen atom into the surface structure itself.

Using a latest and more accurate PES, new MD simulations for oxygen atom recombination on  $\beta$ -cristobalite via the ER mechanism [82] were presented. The updated recombination coefficients compare well with those reported in [72] and with the experimental data reported in [246]. It is worth noting that, as evident in Figure 6 of Ref. [82], the experimental recombination coefficient  $\gamma_{\text{O}}$  reported in the literature as a function of the gas temperature and the surface temperature exhibits a large spread due to the different conditions of the catalytic system considered in

the experiments and in the simulations. The new calculations [82] confirm the non-Boltzmann behaviour of vibrational distributions of the  $O_2$  molecules formed in the ER atom recombination reaction: at low  $E_{kin}$ , the distributions exhibit a sharp peak for  $v = 0$  followed by a large band centred around  $v = 20$ . At higher  $E_{kin}$ , the vibrational distributions are broader with more than a maximum.

In Ref. [80] a very accurate PES, based on ab initio electronic structure calculations, was obtained as a first step to characterise the dynamics of nitrogen atoms recombination on silica surface. In particular, was studied the N/ $N_2$  interaction with a Si atom on silica model clusters, by calculating the interaction potential of the N( $N_2$ )- $SiO_2$  system along the  $C_2$  ( $C_{2v}$  molecular) symmetry axis by keeping the  $SiO_2$  geometry fixed at the experimental values of the  $\beta$ -cristobalite unit cell. The more realistic N/ $N_2$ - $Si_xO_yH_z$  heterogeneous system of the  $\beta$ -cristobalite was also considered and the corresponding calculated interaction potential was assumed in MD simulation of the ER recombination reaction of N atoms on the silica surface. The calculated  $\gamma_N$  was 0.04, while the energy transferred to the surface is nearly 40% of reaction exothermicity mainly for low collisional energy, while at higher values of  $E_{kin}$  nitrogen molecules are formed with high translational energy. The energy partitioning of the exothermic energy released in the recombination reaction between the internal degrees of freedom of the formed  $N_2$  molecules (vibration, rotation, translation) and the surface, shows that the recombination process promotes the population from the bottom of the vibrational ladder with a maximum peak at  $v = 0$ .

The dynamics of hydrogen atom recombination on  $\beta$ -cristobalite has been studied in detail in [81] using the semiclassical MD approach and a potential energy surface, based on DFT calculations (see Ref. [247] for details). The probabilities for the different atomic and molecular surface processes were determined as a function of several parameters: surface temperature (300 K and 1000 K), kinetic energy (0.04-3.0 eV) and incident angles ( $0^\circ$ ,  $45^\circ$ ) of the gas-phase H atom impinging the silica surface. The atomic recombination dynamics was studied in detail by determining the energetics and the ro-vibrational distributions of the formed  $H_2$  molecules obtained for the different dynamics conditions. The recombination coefficients were also obtained for the different initial conditions. In Figure 24 the recombination coefficients,  $\gamma_i$ , for  $T_S = 1000$  K for H, O and N recombination on  $\beta$ -cristobalite surface are reported for comparison [81, 82, 80]. It appears that for O and N recombination  $\gamma_i$  decreases as the gas temperature increases, the contrary occurring for H recombination. Overall, the  $\gamma_O$  is the lowest coefficient in the complete range of considered gas temperatures.

In Figure 25 the vibrational population distributions for H, O and N atoms recombination on silica surface for  $E_{kin} = 0.05$  eV and  $T_S = 1000$  K as obtained in Refs. [81, 82, 80] are reported. Looking to the figure we can immediately infer the non-Boltzmann behaviour of vibrational distributions, in particular in the case of nitrogen molecules recombine mainly in the lowest vibrational level.

Other important series of studies have also been performed for O/ $O_2$  reactant mixtures over graphite basal surface, which was taken as a model for carbon-based TPSs. A first study [248] used DFT calculations to characterize all stationary points (*i.e.*, minima and transition states) involved in the different heterogeneous elementary processes. Atomic sticking was an activated process, whose energy barrier decreased for lower coverage and under slab relaxation. The O adsorption was mostly produced on C-C bridge sites with a considerable puckering of these carbon atoms. Oxygen recombination via ER and LH processes was also activated processes although their energy barriers decrease with coverage increment, especially for ER reaction, which

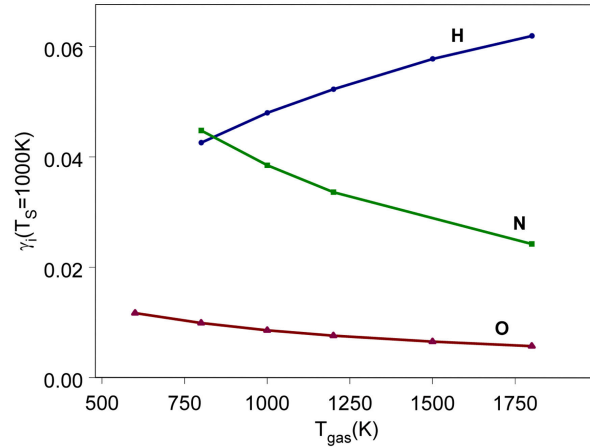


Figure 24: Recombination coefficients  $\gamma_i$  for H, O and N on  $\beta$ -cristobalite, as obtained in Refs. [81, 82, 80].

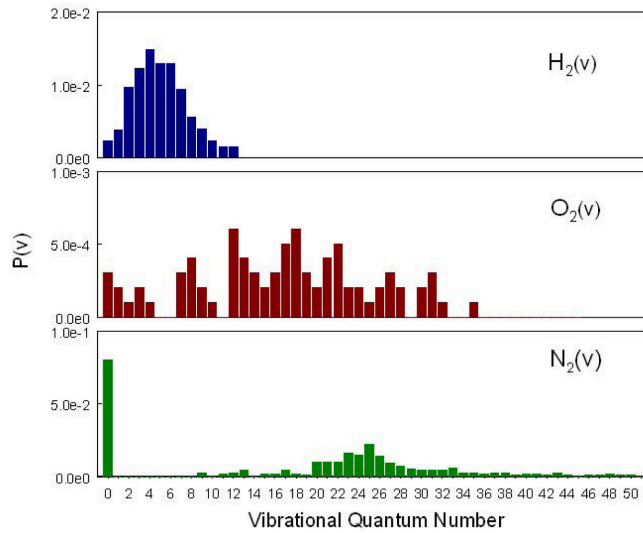


Figure 25: Vibrational population distributions of the  $\text{H}_2$ ,  $\text{O}_2$  and  $\text{N}_2$  molecules formed on silica surface for  $E_{\text{kin}} = 0.05 \text{ eV}$ ,  $T_S = 1000 \text{ K}$ .

dominates the atomic recombination reaction from low to high temperatures because its much lower energy barrier. The application of a microkinetic model with six elementary processes and thermal rate constants derived by using the Transition State Theory (TST) showed a very low oxygen recombination coefficient ( $\gamma_{\text{O}} < 5 \cdot 10^{-4}$ ) within the interval 300 K-900 K. Moreover, it was confirmed a very small contribution of the LH reaction and a very low atomic coverage, which along with the small rate constants allow to explain the low atomic recombination coefficients arising mainly

from the ER reaction.

Classical dynamics studies for O [249, 74] and O<sub>2</sub> [250] over clean and O-precovered graphite surfaces were also made with analytical PESs based on DFT data with different collision energies (0.01-2 eV), surface temperatures (100 K-900 K) and incident angles (0°, 45°). In the first case, was verified that atomic sticking occurs predominantly over bridge sites with low probabilities, in agreement with previous study [248]. The analysis of the distributions of the energy transferred by the reflected atoms to the surface indicated a significant release from the colliding atom to the surface, which was more important for higher atomic collision energies. The collision of O over an O-precovered graphite surface [74] indicated that ER reaction and O reflection were the main processes in agreement with earlier experimental and theoretical studies [248], becoming the ER mechanism more important than the O reflection for normal incidence and with an opposite behaviour for off normal incidence. Moreover, molecular oxygen formed via ER reaction was translationally and internally excited. Finally, the QCT study of molecular oxygen colliding over graphite surface for some ro-vibrational O<sub>2</sub> levels ( $v = 0,1,2$  and  $j = 1,17,25$ ) [250] presented only O<sub>2</sub> reflection even at high collision energies and vibrational excitation, in agreement with the low expected molecular dissociation. The reflected molecules lose mainly collision energy (*i.e.*, not internal), which is primarily transferred to the surface. The calculation of  $\gamma_O$  and  $\beta_O$  coefficients for an O/O<sub>2</sub> gas mixture reacting over graphite could also be made in a similar way as for  $\beta$ -cristobalite [73] by using the dynamical data instead of TST data obtained for the different mentioned studies on the elementary processes, but it is still missing. This study supported

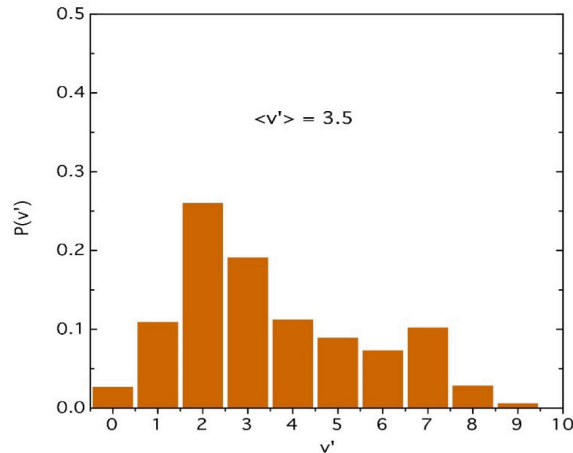


Figure 26: QCT final vibrational CO( $v'$ ) distribution of reflected CO( $v=2$ ,  $j=0$ ) molecules colliding over O-precovered  $\beta$ -cristobalite surface for normal incidence,  $E_{kin} = 0.5$  eV and surface temperature of 300 K. The distribution shown is normalized to population unity. Average final vibrational value is also indicated.

that O + O processes should be much more important than CO+O ones over silica-based surfaces for similar initial conditions of reactants, whose principal processes (O sticking and O<sub>2ads</sub> formation) can release predominantly their energy to the surface (Figure 27). Mars atmosphere contains about 95% carbon dioxide and during the entry of space vehicles into this atmosphere at high collision energies (*i.e.*, about 4.5

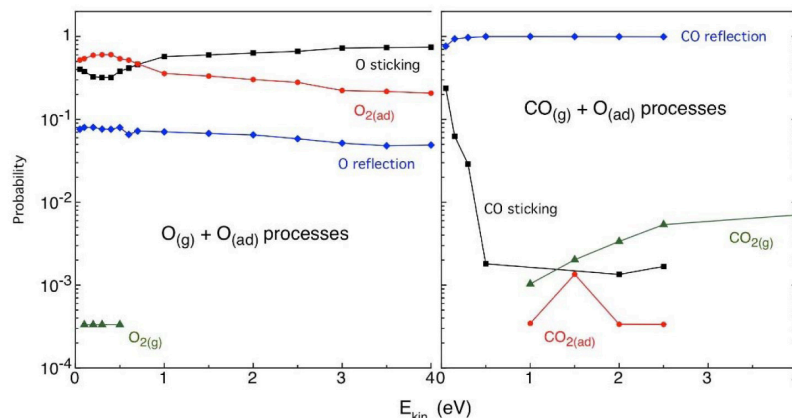


Figure 27: QCT reaction probabilities for an O-precovered  $\beta$ -cristobalite surface at several collision energies, with normal incidence and at surface temperature of 300 K for two gas species: a) O and b)  $\text{CO}(v=0, j=0)$ .

$\pm 1.0$  eV) produces mainly the breaking of  $\text{CO}_2$  molecules into  $\text{CO} + \text{O}$ . Experimental investigation about carbon monoxide and oxygen mixtures on quartz seems to indicate that oxygen recombination should be more important than CO oxidation in the range of pressures and temperatures studied [251]. On the other hand, CO molecules can react over an O-preadsorbed silica surface to produce atomic reflection and adsorption along with  $\text{CO}_2$  formation, probably via an ER recombination mechanism that should be more likely than a LH mechanism. A recent study has been performed to ascertain the importance of the  $\text{CO} + \text{O}$  elementary processes in comparison with the  $\text{O} + \text{O}$  ones to shed light to this point [93]. In this work was carried out a QCT study for carbon monoxide collisions over an oxygen preadsorbed  $\beta$ -cristobalite surface by using a based reactive force field (ReaxFF) PES. The collisions were performed fixing several initial conditions: CO ro-vibrational states ( $v=0-5$  and  $j=0, 20, 35$ ), collision energies (0.05-2.5 eV), incident angles ( $0^\circ, 45^\circ$ ) and surface temperatures (300 K and 900 K). The main elementary processes were the molecular reflection and the non-dissociative molecular adsorption (sticking).  $\text{CO}_2$  molecules were also formed in minor extension via an ER mechanism although some of them were finally adsorbed on the surface. The scattered (reflected) CO molecules were translationally colder and internally hotter (rotationally and vibrationally) than the initial ones. The effect of the initial collision energy on these  $\text{CO}(v')$  final distributions was small, which show a bimodal shape for initial CO molecules with  $v > 2$  and for all collision energies studied (Figure 26).

## 5. Conclusions and perspectives

The relevance of advanced StS kinetic models, including accurate and detailed dynamical information, in the reliable description of non-equilibrium conditions characterizing the high-speed entry in Earth atmosphere is nowadays well-assessed in the modeling community. A predictive theoretical model could assist the designing of TPS and the choice of new materials, based on the fundamental knowledge acquired

on the role of excited species in the plasma in the shock region, on the catalytic response of surfaces and on the microscopic collisional mechanisms driving the plasma evolution. The StS approach has triggered an intense research activity aiming to the theoretical investigation of the molecular dynamics of the elementary processes relevant to the plasma kinetics that, dealing with complete dataset ro-vibrationally resolved and in some cases also with processes involving electronically excited species, benefits significantly from the possibilities offered by modern web-access databases for the collection, validation and distribution of dynamical results. This review focuses on the most recent efforts done in the derivation of accurate, complete and consistent state-resolved cross sections and rate coefficients for inelastic and reactive channels, belonging to the **four** main classes of processes, namely electron-molecule, atom-molecule, molecule-molecule and atom/molecule-surface, and involving the chemical species relevant to Earth ( $\text{N}_2, \text{O}_2, \text{NO}$ ), Mars ( $\text{CO}_2, \text{CO}, \text{N}_2$ ) and Jupiter ( $\text{H}_2, \text{He}$ ) atmospheres.

The creation of this new database for the modeling of re-entry conditions in planetary atmospheres can be regarded as a step forward in the actual practicability of StS kinetics, and in the understanding the role of the collisional dynamics in affecting the macroscopic quantities characterizing the plasma.

Data validation is performed by comparison with experimental results available in literature. A comprehensive discussion, limited to the ground or, in the luckiest cases, to the first few vibrational levels, for data here reviewed can be found in the original papers and also in the phys4entry database [19]. A general satisfactory agreement is observed.

However it should be stressed that there are issues still to be addressed, *i.e.* the detailed vibrational kinetics for tri-atomic molecules, accounting for the complex multi-mode vibrational structure and the dynamical characterization of the inter-mode coupling, the role of non-adiabatic coupling (conical intersection) among different electronic states, resulting in multi-surface dynamics, and the possible role of excited species in heavy particle collisions, **not to mention the role of electronically excited states in the development of collisional-radiative models.**

All these problems need attention and represent the future challenges for the molecular dynamic community.

## Acknowledgments

The research leading to these results has received funding from the European Community's Seventh Framework Programme (FP7/2007-2013) under grant agreement n. 242311. R. Sayós and P. Gamallo received partial financial support by the Spanish MINECO CTQ2014-53987-R project and from the Generalitat de Catalunya 2014SGR1582 project. M. Rutigliano received also partially support from MIUR (PRIN2010ERFKXL\_008). A. Laganà and A. Lombardi thank the VII FP (Egi-Inspire), the COST (Action CM901), the Dipartimento di Chimica, Biologia e Biotecnologie di Perugia and the "Fondazione Cassa Risparmio Perugia (Codice Progetto: 2015.0331.021 Ricerca Scientifica e Tecnologica)". A. Lombardi gratefully acknowledges financial support by Italian MIUR (PRIN 2010-2011, grant 2010ERFKXL), and allocated computing time by the Virtual Organization COMPChem and the OU Supercomputing Center for Education & Research (OSCER) at the University of Oklahoma (OU).

## References

- [1] Park C (ed) 2012 *Nonequilibrium Hypersonic Aerothermodynamics* (Wiley)
- [2] Colonna G, Armenise I, Bruno D and Capitelli M 2006 *Journal of Thermophysics and Heat Transfer* **20** 477–486
- [3] Colonna G, Pietanza L D and Capitelli M 2008 *Journal of Thermophysics and Heat Transfer* **22** 399–406
- [4] Guy A, Bourdon A and Perrin M Y 2013 *Chemical Physics* **420** 15–24
- [5] Capitelli M (ed) 1986 *Nonequilibrium Vibrational Kinetics in Springer Series Topics in Current Physics* vol 39 (Springer)
- [6] Loureiro J, Guerra V, Sá P A, Pintassilgo C D and Lino da Silva M 2011 *Plasma Sources Science and Technology* **20** 024007
- [7] Capitelli M, Celiberto R, Colonna G, Esposito F, Gorse C, Hassouni K, Laricchiuta A and Longo S 2015 *Fundamental Aspects of Plasma Chemical Physics: Kinetics* (Springer Series on Atomic, Optical, and Plasma Physics)
- [8] Nagnibeda E and Kustova E 2009 *Non-Equilibrium Reacting Gas Flows: Kinetic Theory of Transport and Relaxation Processes in Springer Series Heat and Mass Transfer* (Berlin Heidelberg: Springer-Verlag)
- [9] Perrin M Y, Rivière P and Soufiani A 2012 *Radiation phenomena behind shock waves in High Temperature Phenomena in Shock Waves R. Brun (ed.)* vol 50 (Springer Verlag)
- [10] Surzhikov S T 2012 *Journal of Heat Transfer* **134** 031002–031002
- [11] Bultel A and Annaloro J 2013 *Plasma Sources Science and Technology* **22** 025008
- [12] Colonna G, D’Ammando G, Pietanza L D and Capitelli M 2015 *Plasma Physics and Controlled Fusion* **57** 014009
- [13] D’Ammando G, Capitelli M, Esposito F, Laricchiuta A, Pietanza L D and Colonna G 2014 *Physics of Plasmas* **21** 093508
- [14] Capitelli M, Colonna G, Pietanza L and D’Ammando G 2013 *Spectrochimica Acta Part B: Atomic Spectroscopy* **83–84** 1–13
- [15] Capitelli M, Armenise I, Bruno D, Cacciatore M, Celiberto R, Colonna G, De Pascale O, Diomede P, Esposito F, Gorse C, Hassouni K, Laricchiuta A, Longo S, Pagano D, Pietanza D and Rutigliano M 2007 *Plasma Sources Science and Technology* **16** S30
- [16] Capitelli M, Cacciatore M, Celiberto R, De Pascale O, Diomede P, Esposito F, Gicquel A, Gorse C, Hassouni K, Laricchiuta A, Longo S, Pagano D and Rutigliano M 2006 *Nuclear Fusion* **46** S260
- [17] Armenise I and Capitelli M 2005 *Plasma Sources Science and Technology* **14** S9
- [18] LXcat 2015 Plasma Data Exchange Project database, <http://fr.lxcat.net/home/>
- [19] 2015 Phys4entry database, <http://users.ba.cnr.it/imip/cscpal38/phys4entry/database.html>
- [20] STELLAR, <http://estheristutlpt/pages/stellarhtml> 2015
- [21] Colonna G and Capitelli M 2008 *Journal of Thermophysics and Heat Transfer* **22** 414–423
- [22] Capitelli M, Armenise I, Bisceglie E, Bruno D, Celiberto R, Colonna G, D’Ammando G, De Pascale O, Esposito F, Gorse C, Laporta V and Laricchiuta A 2012 *Plasma Chemistry and Plasma Processing* **32** 427–450
- [23] Panesi M, Jaffe R L, Schwenke D W and Magin T E 2013 *The Journal of Chemical Physics* **138** 044312
- [24] Capitelli M, Colonna G, D’Ammando G, Laporta V and Laricchiuta A 2014 *Chemical Physics* **438** 31–36
- [25] Munafò A and Magin T E 2014 *Physics of Fluids* **26** 097102
- [26] Armenise I and Esposito F 2015 *Chemical Physics* **446** 30–46
- [27] Armenise I, Esposito F and Capitelli M 2007 *Chemical Physics* **336** 83–90
- [28] Armenise I and Esposito F 2012 *Chemical Physics, special issue Chemical Physics of Low-Temperature Plasmas (in honour of Prof Mario Capitelli)* **398** 104–110
- [29] Loureiro J, Ferreira C M, Capitelli M, Gorse C and Cacciatore M 1990 *Journal of Physics D: Applied Physics* **23** 1371
- [30] Colonna G, Laporta V, Celiberto R, Capitelli M and Tennyson J 2015 *Plasma Sources Science and Technology* **24** 035004
- [31] Laporta V, Celiberto R and Tennyson J 2013 *Plasma Sources Science and Technology* **22** 025001
- [32] Laporta V, Celiberto R and Wadehra J M 2012 *Plasma Sources Science and Technology* **21** 055018
- [33] Laporta V, Cassidy C M, Tennyson J and Celiberto R 2012 *Plasma Sources Science and Technology* **21** 045005

- [34] Laporta V, Little D A, Celiberto R and Tennyson J 2014 *Plasma Sources Science and Technology* **23** 065002
- [35] Laporta V, Celiberto R and Tennyson J 2015 *Physical Review A* **91**(1) 012701
- [36] Capitelli M and Celiberto R 1998 *Novel Aspects of Electron-Molecule Collisions* (K. H. Becker (Ed.)) pp 283–323
- [37] Laricchiuta A, Celiberto R and Capitelli M 2000 *Chemical Physics Letters* **329** 526–532
- [38] Celiberto R, Janev R, Laricchiuta A, Capitelli M, Wadehra J and Atems D 2001 *Atomic Data and Nuclear Data Tables* **77** 161–213
- [39] Kosarim A, Smirnov B, Capitelli M, Celiberto R, Petrella G and Laricchiuta A 2005 *Chemical Physics Letters* **414** 215–221
- [40] Laricchiuta A, Capitelli M, Celiberto R and Colonna G 2006 *37th AIAA Plasmadynamics and Lasers Conference, San Francisco, California (USA), June 5-8 2006, AIAA-2006-2898*
- [41] Kosarim A, Smirnov B, Capitelli M, Celiberto R, Laricchiuta A and Panicia F 2006 *Chemical Physics Letters* **422** 513–517
- [42] Esposito F, Armenise I and Capitelli M 2006 *Chemical Physics* **331** 1–8
- [43] Caridade P J S B, Galvão B R L and Varandas A J C 2010 *The Journal of Physical Chemistry A* **114** 6063–6070
- [44] Akpinar S, Armenise I, Defazio P, Esposito F, Gamallo P, Petrongolo C and Sayós R 2012 *Chemical Physics* **398** 81–89
- [45] Laganà A and Garcia E 2015 *VIRT&L-COMM* **5** 5–2014.10
- [46] Laganà A, de Aspuru G O and Garcia E 2015 *VIRT&L-COMM* **5** 5–2014.11
- [47] Laganà A, Garcia E and Martínez T 2014 *VIRT&L-COMM* **5** 5–2014.12
- [48] Andrienko D and Boyd I D 2015 *Chemical Physics* **459** 1–13
- [49] Richard Jaffe, David Schwenke and Galina Chaban 2009 *AIAA-Paper 2009-1569*
- [50] Bose D and Candler G V 1997 *The Journal of Chemical Physics* **107** 6136–6145
- [51] Bose D and Candler G V 1996 *The Journal of Chemical Physics* **104** 2825–2833
- [52] Billing G 1986 *Nonequilibrium Vibrational Kinetics* (Ed. M. Capitelli) **39**
- [53] Capitelli M, Gorse C and Billing G 1980 *Chemical Physics* **52** 299–304
- [54] Cacciatore M, Kurnosov A and Napartovich A 2005 *J. Chem. Phys.* **123** 174315
- [55] Kurnosov A, Cacciatore M, Laganà A, Pirani F, Bartolomei M and Garcia E 2014 *Journal of Computational Chemistry* **35** 722–736
- [56] Kurnosov A K, Napartovich A P, Shnyrev S L and Cacciatore M 2010 *Plasma Sources Science and Technology* **19** 045015
- [57] Garcia E, Martínez T and Laganà A 2015 *Chemical Physics Letters* **620** 103–108
- [58] Adamovich I V, MacHeret S O, Rich J W and Treanor C E 1998 *Journal of Thermophysics and Heat Transfer* **12** 57–65
- [59] Lino da Silva M, Guerra V and Loureiro J 2009 *Plasma Sources Science and Technology* **18** 034023
- [60] Lino da Silva M, Loureiro J and Guerra V 2012 *Chemical Physics Letters* **531** 28–33
- [61] Coletti C and Billing G 2002 *Chemical Physics Letters* **356** 14–22
- [62] Bender J D, Valentini P, Nompelis I, Pauku Y, Varga Z, Truhlar D G, Schwartzentruber T and Candler G V 2015 *The Journal of Chemical Physics* **143** 054304
- [63] Valentini P, Schwartzentruber T E, Bender J D, Nompelis I and Candler G V 2015 *Physics of Fluids* **27** 086102
- [64] Esposito F and Capitelli M 2009 *The Journal of Physical Chemistry A* **113** 15307–15314
- [65] Forrey R C 2013 *Phys. Rev. A* **88**(5) 052709
- [66] Muiño R D and Busnengo H F (eds) 2013 *Dynamics of Gas-Surface Interactions: atomic-level understanding of scattering processes at surface* vol 50 (Springer Series in Surface Science)
- [67] Cacciatore M and Rutigliano M 2009 *Plasma Sources Science and Technology* **18** 023002
- [68] Armenise I, Barbato M, Capitelli M and Kustova E 2006 *Journal of Thermophysics and Heat Transfer* **20** 465–476
- [69] Armenise I, Rutigliano M, Cacciatore M and Capitelli M 2011 *Journal of Thermophysics and Heat Transfer* **25** 627–632
- [70] Armenise I and Kustova E V 2014 *Chemical Physics* **428** 90 – 104
- [71] Molinari E and Tomellini M 2006 *Catalysis Today* **116** 30–37
- [72] Arasa C, Morón V, Busnengo H F and Sayós R 2009 *Surface Science* **603** 2742–2751
- [73] Morón V, Gamallo P, Martin-Gondre L, Crespos C, Larregaray P and Sayós R 2011 *Physical Chemistry Chemical Physics* **13** 17494
- [74] Morón V, Martin-Gondre L, Gamallo P and Sayós R 2012 *The Journal of Physical Chemistry C* **116** 13092–13103
- [75] Bedra L, Rutigliano M, Balat-Pichelin M and Cacciatore M 2006 *Langmuir* **22** 7208–7216

- [76] Cacciatore M, Rutigliano M and Billing G D 1999 *Journal of Thermophysics and Heat Transfer* **13** 195–203
- [77] Cacciatore M 1999 *Pure and Applied Chemistry* **71** 1809–1817
- [78] Rutigliano M, Zazza C, Sanna N, Pieretti A, Mancini G, Barone V and Cacciatore M 2009 *The Journal of Physical Chemistry A* **113** 15366–15375
- [79] Zazza C, Rutigliano M, Sanna N, Barone V and Cacciatore M 2012 *The Journal of Physical Chemistry A* **116** 1975–1983
- [80] Rutigliano M, Pieretti A, Cacciatore M, Sanna N and Barone V 2006 *Surface Science* **600** 4239–4246
- [81] Rutigliano M, Gamallo P, Sayós R, Orlandini S and Cacciatore M 2014 *Plasma Sources Science and Technology* **23** 045016
- [82] Rutigliano M and Cacciatore M 2015 *Journal of Thermophysics and Heat Transfer* (in press)
- [83] Celiberto R, Janev R K, Wadehra J M and Laricchiuta A 2008 *Physical Review A* **77** 012714
- [84] Celiberto R, Janev R K, Wadehra J M and Laricchiuta A 2009 *Physical Review A* **80** 012712
- [85] Capitelli M, Celiberto R, Colonna G, D’Ammando G, De Pascale O, Diomede P, Esposito, Gorse C, Laricchiuta A, Longo S and Pietanza L D 2010 *J. Phys. B: At. Mol. Opt. Phys.* **43** 144025
- [86] Celiberto R, Janev R K, Wadehra J M and Laricchiuta A 2011 *Physical Review A* **84** 012707
- [87] Celiberto R, Janev R K, Laporta V, Tennyson J and Wadehra J M 2013 *Physical Review A* **88** 062701
- [88] Armenise I and Kustova E 2013 *Chemical Physics* **415** 269–281
- [89] Kozák T and Bogaerts A 2014 *Plasma Sources Science and Technology* **23** 045004
- [90] Taylan O and Berberoglu H 2015 *Plasma Sources Science and Technology* **24** 015006
- [91] Celiberto R, Laporta V, Laricchiuta A, Wadehra J and Tennyson J 2014 *The Open Plasma Physics Journal* **7** 33–47
- [92] Lombardi A, Faginas-Lago N, Pacifici L and Costantini A 2013 *The Journal of Physical Chemistry A* **117** 11430–11440
- [93] Gamallo P, Prats H and Says R 2014 *Journal of Molecular Modeling* **20** 2160
- [94] Laganà A, Lombardi A, Pirani F, Gamallo P, Sayós R, Armenise I, Cacciatore M, Esposito F and Rutigliano M 2014 *The Open Plasma Physics Journal* **7** 48–59
- [95] Pietanza L D, Colonna G, D’Ammando G, Laricchiuta A and Capitelli M 2015 *Plasma Sources Science and Technology* **24** 042002
- [96] Gryziński M 1965 *Phys. Rev.* **138**(2A) A336–A358
- [97] Chung S and Lin C C 1972 *Phys. Rev. A* **6**(3) 988–1002
- [98] Hazi A U 1981 *Phys. Rev. A* **23**(5) 2232–2240
- [99] Redmon M J, Garrett B C, Redmon L T and McCurdy C W 1985 *Phys. Rev. A* **32**(6) 3354–3365
- [100] Celiberto R and Rescigno T N 1993 *Phys. Rev. A* **47**(3) 1939–1945
- [101] Kim Y K 2007 *The Journal of Chemical Physics* **126** 064305
- [102] Adamson S, Astapenko V, Deminskii M, Eletsii A, Potapkin B, Sukhanov L and Zaitsevskii A 2007 *Chemical Physics Letters* **436** 308–313
- [103] Kim Y K and Rudd M E 1994 *Phys. Rev. A* **50**(5) 3954–3967
- [104] Nishimura H and Danjo A 1986 *Journal of the Physical Society of Japan* **55** 3031–3036
- [105] Khakoo M A, Trajmar S, McAdams R and Shyn T W 1987 *Phys. Rev. A* **35**(7) 2832–2837
- [106] Khakoo M A and Segura J 1994 *Journal of Physics B: Atomic, Molecular and Optical Physics* **27** 2355
- [107] Stibbe D T and Tennyson J 1998 *New Journal of Physics* **1** 2
- [108] Trevisan C S and Tennyson J 2002 *Plasma Physics and Controlled Fusion* **44** 1263
- [109] Rescigno T N and Schneider B I 1988 *Journal of Physics B: Atomic, Molecular and Optical Physics* **21** L691
- [110] Celiberto R, Capitelli M and Laricchiuta A 2002 *Physica Scripta* **2002** 32
- [111] Liu X, Shemansky D E, Johnson P V, Malone C P, Khakoo M A and Kanik I 2012 *Journal of Physics B: Atomic, Molecular and Optical Physics* **45** 015201
- [112] Laricchiuta A, Celiberto R and Janev R K 2004 *Phys. Rev. A* **69**(2) 022706
- [113] Wunderlich D 2011 *Chemical Physics* **390** 75–82
- [114] Celiberto R, Baluja K L, Janev R K and Laporta V 2015 *Plasma Physics and Controlled Fusion* **58** 014024
- [115] Cosby P C 1993 *The Journal of Chemical Physics* **98** 9544–9553
- [116] Capitelli M, Celiberto R, Eletsii A and Laricchiuta A 2001 *Atomic and Plasma-Material Interaction Data for Fusion* **9** 47–64
- [117] Wakiya K 1978 *Journal of Physics B: Atomic and Molecular Physics* **11** 3913
- [118] Suzuki D, Kato H, Ohkawa M, Anzai K, Tanaka H, Limô-Vieira P, Campbell L and Brunger

- M J 2011 *The Journal of Chemical Physics* **134** 064311
- [119] Stahel D, Leoni M and Dressler K 1983 *Journal of Chemical Physics* **79** 2541–2558
- [120] Spelsberg D and Meyer W 2001 *Journal of Chemical Physics* **115** 6438–6449
- [121] Gibson S T and Lewis B R 1996 *Journal of Electron Spectroscopy and Related Phenomena* **80** 9–12
- [122] Lewis B R, England J P, Gibson S T, Brunger M J and Allan M 2001 *Phys. Rev. A* **63**(2) 022707
- [123] Khakoo M A, Malone C P, Johnson P V, Lewis B R, Laher R, Wang S, Swaminathan V, Nuyujukian D and Kanik I 2008 *Physical Review A* **77** 012704
- [124] Malone C P, Johnson P V, Liu X, Ajdari B, Kanik I and Khakoo M A 2012 *Physical Review A* **85**(6) 062704
- [125] Straub H C, Renault P, Lindsay B G, Smith K A and Stebbings R F 1996 *Phys. Rev. A* **54**(3) 2146–2153
- [126] Krishnakumar E and Srivastava S K 1990 *Journal of Physics B: Atomic, Molecular and Optical Physics* **23** 1893
- [127] Shemansky D E and Liu X 2005 *Journal of Geophysical Research: Space Physics* **110** A07307
- [128] Cacciatore M, Capitelli M and Gorse C 1982 *Chemical Physics* **66** 141–151
- [129] Van Zyl B and Pendleton W 1995 *Journal of Geophysical Research: Space Physics* **100** 23755–23762
- [130] Doering J P and Yang J 1997 *Journal of Geophysical Research: Space Physics* **102** 9691–9696
- [131] Stibbe D T and Tennyson J 1998 *J. Phys. B: At. Mol. Opt. Phys.* **31** 815–844
- [132] Allan M 1985 *J. Phys. B: At. Mol. Opt. Phys.* **18** 4511
- [133] Noble C J, Higgins K, Wöste G, Duddy P, Burke P G, Teubner P J O, Middleton A G and Brunger M J 1996 *Phys. Rev. Lett.* **76** 3534–3537
- [134] Allan M 1995 *Journal of Physics B: Atomic, Molecular and Optical Physics* **28** 5163
- [135] Wong S F, Boness M J W and Schulz G J 1973 *Phys. Rev. Lett.* **31** 969–972
- [136] Laporta V, Celiberto R and Tennyson J 2014 *AIP Conference Proceedings* **1628** 939–942
- [137] Trevisan C S, Houfek K, Zhang Z, Orel A E, McCurdy C W and Rescigno T N 2005 *Phys. Rev. A* **71** 052714
- [138] Allan M 2005 *J. Phys. B: At. Mol. Opt. Phys.* **38** 603
- [139] Allan M 2004 *Journal of Physics B: Atomic, Molecular and Optical Physics* **37** L359–L363
- [140] Nandi D, Prabhudesai V S, Nestmann B M and Krishnakumar E 2011 *Physical Chemistry Chemical Physics* **13** 1542–1551
- [141] Laporta V, Celiberto R and Tennyson J 2015 *Plasma Sources Science and Technology, Fast Track Communication (submitted)*
- [142] Allan M 2010 *Phys. Rev. A* **81**(4) 042706
- [143] Bardsley J N and Wadehra J M 1979 *Phys. Rev. A* **20**(4) 1398–1405
- [144] Horáček J, Čížek M, Houfek K, Kolorenč P and Domcke W 2006 *Phys. Rev. A* **73**(2) 022701
- [145] Schulz G J 1973 *Rev. Mod. Phys.* **45** 423–486
- [146] Wadehra J M and Bardsley J N 1978 *Phys. Rev. Lett.* **41**(26) 1795–1798
- [147] Wadehra J M 1979 *Appl. Phys. Lett.* **35** 917
- [148] Atoms D E and Wadehra J M 1990 *Phys. Rev. A* **42** 5201
- [149] Horáček J, Čížek M, Houfek K, Kolorenč P and Domcke W 2004 *Phys. Rev. A* **70**(5) 052712
- [150] Atoms D E and Wadehra J M 1993 *Journal of Physics B: Atomic, Molecular and Optical Physics* **26** L759
- [151] Celiberto R, Janev R, Wadehra J and Tennyson J 2012 *Chemical Physics, Special Issue Chemical Physics of Low-Temperature Plasmas (in honour of Prof Mario Capitelli)* **398** 206–213
- [152] Comer J and Read F H 1971 *J. Phys. B* **4** 368
- [153] Houfek K, Rescigno T N and McCurdy C W 2006 *Phys. Rev. A* **73**(3) 032721
- [154] Huo W M, Gibson T L, Lima M A P and McKoy V 1987 *Phys. Rev. A* **36** 1632–1641
- [155] Tennyson J 2010 *Physics Reports* **491** 29–76
- [156] Domcke W 1991 *Physics Reports* **208** 97–188
- [157] Burke P G 2011 *R-Matrix Theory of Atomic Collisions: Application to Atomic, Molecular and Optical Processes* (Springer)
- [158] Tennyson J 1996 *Journal of Physics B: Atomic, Molecular and Optical Physics* **29** 1817–1828
- [159] Tennyson J and Noble C J 1984 *Computer Physics Communications* **33** 421–424
- [160] Stibbe D T and Tennyson J 1996 *Journal of Physics B: Atomic, Molecular and Optical Physics* **29** 4267–4283
- [161] Berman M, Estrada H, Cederbaum L S and Domcke W 1983 *Phys. Rev. A* **28** 1363–1381
- [162] Mündel C, Berman M and Domcke W 1985 *Physical Review A* **32** 181

- [163] Nestmann B M, Kumar S V K and Peyerimhoff S D 2005 *Physical Review A* **71** 012705
- [164] Little D A and Tennyson J 2014 *Journal of Physics B: Atomic, Molecular and Optical Physics* **47** 105204
- [165] Little D A and Tennyson J 2013 *Journal of Physics B: Atomic, Molecular and Optical Physics* **46** 145102
- [166] Werner H J, Knowles P J, Knizia G, Manby F R and Schütz M 2012 *WIREs Comput. Mol. Sci.* **2** 242–253
- [167] Spence D and Burrow P D 1979 *J. Phys B: Atom. Molec. Phys.* **12** L179
- [168] Huetz A, Gresteau F, Hall R I and Mazeau J 1980 *The Journal of Chemical Physics* **72** 5297–5304
- [169] Huetz A, Gresteau F and Mazeau J 1980 *Journal of Physics B: Atomic and Molecular Physics* **13** 3275
- [170] Fabrikant I I, Wadhera J M and Xu Y 2002 *Physica Scripta* **2002** 45
- [171] Bieniek R J and Dalgarno A 1979 *The Astrophysical Journal* **228** 635
- [172] Kreckel H, Bruhns H, ek M, Glover S C O, Miller K A, Urbain X and Savin D W 2010 *Science* **329** 69
- [173] Sheehan C H and St-Maurice J P 2004 *Journal of Geophysical Research* **109** A03302
- [174] Little D A, Chakrabarti K, Mezei J Z, Schneider I F and Tennyson J 2014 *Physical Review A* **90** 052705
- [175] Larsson M and Orel A E 2008 *Dissociative Recombination of Molecular Ions* (Cambridge University Press)
- [176] 2013 *Proceedings of Ninth International Conference on Dissociative Recombination: Theory, Experiment and Applications (DR2013). July 2013, Paris, France. I.F. Schneider, O. Dulieu and J. Robert (Eds.)*
- [177] Hutson J M and Green S 1994 Molscat computer code
- [178] Hase W L, Duchovic R J, Hu X, Komornicki A, Lim K F, Lu D, Peshherbe G H, Swamy K N, Vande Linde S R, Zhu L, Varandas A, Wang H and Wolf R J 1996 *J. Quantum Chemistry Program Exchange Bulletin* **16** 671
- [179] Billing G 1984 *Computer Physics Reports* **1** 239–296
- [180] De Fazio D 2014 *Phys. Chem. Chem. Phys.* **16**(23) 11662–11672
- [181] Gervasi O, Manuali C, Laganà A and Costantini A 2009 *Chemistry and Material Science Applications on Grid Infrastructures. ICTP Lecture Notes* **24** 63–82
- [182] Maitland G C, Rigby M, Smith E B and Wakeham W A 1987 *Intermolecular Forces* (Clarendon Press: Oxford)
- [183] Nasri S, Ajili V, Jaidane N, Kalugina Y N, Halvick P, Stoecklin T and Hochlaf H 2015 *J. Chem. Phys.* **142** 174301
- [184] Bartolomei M, Pirani F, Laganà A and Lombardi A 2012 *J. Comp. Chem.* **33** 1806–1819
- [185] Laganà A and Riganelli A 2000 *Fitting Potential Energy Surfaces in Reaction and Molecular dynamics in Lecture Notes in Chemistry, G. C. Schatz (Ed.)* vol 14 (Springer Verlag)
- [186] Garcia E and Laganà A 1985 *Mol. Phys.* **56** 629–639
- [187] Garcia E and Laganà A 1985 *Mol. Phys.* **56** 621–627
- [188] Garcia E, Sanchez C, Rodriguez A and Laganà A 2006 *Int. J. Quantum Chemistry* **106** 623–630
- [189] Rodriguez A, Garcia E, Hernandez M and Laganà A 2012 *Chem. Phys. Lett.* **360** 304–312
- [190] Garcia E, Kurnosov A, Laganà A, Pirani F, Bartolomei M and Cacciatore M 2015 *J. Phys. Chem. B.* (in press)
- [191] Lombardi A, Faginas-Lago N, Pacifici L and Grossi G 2015 *J. Chem. Phys.* **143** 034307
- [192] Lombardi A, Faginas-Lago N and Laganà A 2014 *Grid Calculation Tools for Massive Applications of Collision Dynamics Simulations: Carbon Dioxide Energy Transfer in Computational Science and Its Applications-ICCSA 2014* vol 8579 (Springer Verlag)
- [193] Lombardi A, Laganà A, Pirani F, Palazzetti F and Faginas-Lago N 2013 *Carbon Oxides in Gas Flows and Earth and Planetary Atmospheres: State-to-State Simulations of Energy Transfer and Dissociation Reactions in Computational Science and Its Applications-ICCSA 2013* (Springer Verlag)
- [194] Billing G D 1976 *The Journal of Chemical Physics* **65** 1–6
- [195] Cacciatore M, Kurnosov A, Napartovich A and Shnyrev A 2004 *J. Phys. B* **37** 3379
- [196] Kurnosov A, Napartovich A, Shnyrev S and Cacciatore M 2007 *J. Phys. Chem.* **111** 7057
- [197] Park H and Slinger T G 1994 *J. Chem. Phys.* **100** 287–300
- [198] Billing G D 1994 *Chem. Phys.* **179** 463–467
- [199] Wang D, Stallcop J R, Huo W M, Dateo C E, Schwenke D W and Partridge H 2003 *The Journal of Chemical Physics* **118** 2186–2189
- [200] Rampino S, Skouteris D, Laganà A, Garcia E and Saracibar A 2009 *Physical Chemistry*

- Chemical Physics* **11** 1752
- [201] Faginas N, naga F H L and Laganà A 2008 *Chemical Physics Letters* **464** 249–255
- [202] Schwartz R N, Slawsky Z I and Herzfeld K F 1952 *The Journal of Chemical Physics* **20** 1591–1599
- [203] Rapp D and Kassal T 1969 *Chemical Reviews* **69** 61102
- [204] Adamovich I V 2014 *Physics of Fluids* **26** 046102
- [205] Lino da Silva M, Guerra V, Loureiro J and Sá P A 2008 *Chemical Physics* **348** 187194
- [206] Parker G A and Pack R T 1978 *The Journal of Chemical Physics* **68** 1585
- [207] Esposito F, Coppola C M and De Fazio D 2015 *Journal of Physical Chemistry A* (in press)
- [208] Laganà A, Garcia E and Ciccarelli L 1987 *Journal of Physical Chemistry* **91** 312–314
- [209] Laganà A and Garcia E 1994 *The Journal of Physical Chemistry* **98** 502–507
- [210] Armenise I, Capitelli M and Gorse C 1996 *Journal of Thermophysics and Heat Transfer* **10** 397
- [211] Armenise I, Capitelli M, Kustova E and Nagnibeda E 1999 *Journal of Thermophysics and Heat Transfer* **13** 210–218
- [212] Esposito F, Armenise I and Capitelli M 2006 *18th Europhysics Conference on the Atomic and Molecular Physics of Ionized Gases (ESCAMPIG XVIII), Europhysics Conference Abstracts, Book of Abstracts* **30G** 173
- [213] Laganà A, de Aspuru G O and Garcia E 1994 *6th Joint Thermophysics and Heat Transfer Conference (1994)*
- [214] Laganà A, Ochoa De Aspuru G and Garcia E 1996 *Dipartimento di Chimica, Università di Perugia Perugia, Italy*
- [215] Esposito F and Capitelli M 2006 *Chemical Physics Letters* **418** 581–585
- [216] Bruno D, Capitelli M, Esposito F, Longo S and Minelli P 2002 *Chemical Physics Letters* **360** 31–37
- [217] Esposito F, Capitelli M and Gorse C 2000 *Chemical Physics* **257** 193–202
- [218] Galvão B R L and Varandas A J C 2009 *The Journal of Physical Chemistry* **113** 14424–14430
- [219] Ernesto G, Amaia S, Gómez-Carrasco S and Laganà A 2008 *Physical Chemistry Chemical Physics* **10**(18) 2552–2558
- [220] Esposito F and Capitelli M 2002 *Chemical Physics Letters* **364** 180–187
- [221] Li Y, Sun Z, Jiang B, Xie D, Dawes R and Guo H 2014 *The Journal of Chemical Physics* **141** 081102
- [222] Varandas A and Pais A 1988 *Molecular Physics* **65** 843–860
- [223] Esposito F and Capitelli M 2007 *Chemical Physics Letters* **443** 222–226
- [224] Esposito F, Armenise I, Capitta G and Capitelli M 2008 *Chemical Physics* **351** 91–98
- [225] Ivanov M V, Schinke R and Mcbane G C 2007 *Molecular Physics* **105** 1183–1191
- [226] Miller W H 1970 *Chemical Physics Letters* **7** 431
- [227] Kustova E V 2001 *Chemical Physics* **270** 177–195
- [228] Capitelli M, Colonna G and Esposito F 2004 *The Journal of Physical Chemistry A* **108** 8930–8934
- [229] Armenise I, Reynier P and Kustova E 2015 *Journal of Thermophysics and Heat Transfer* (in press)
- [230] Lowke J J, Phelps A V and Irwin B W 1973 *Journal of Applied Physics* **44** 4664–4671
- [231] Phelps A V 2015
- [232] Pietanza L D, Colonna G, D’Ammando G, Laricchiuta A and Capitelli M 2015 *in preparation*
- [233] Fridman A 2012 *Plasma Chemistry* (Cambridge University Press)
- [234] Rescigno T N, Isaacs W A, Orel A E, Meyer H D and McCurdy C W 2002 *Phys. Rev. A* **65**(3) 032716
- [235] Kustova E V, Nagnibeda E A and Armenise I 2014 *The Open Plasma Physics Journal* **7** 76–87
- [236] Kozák T and Bogaerts A 2015 *Plasma Sources Science and Technology* **24** 015024
- [237] Laub B and Venkatapathy E 2003 *Proceedings of the International Workshop on Planetary Entry and Descent Trajectory Analysis and Science, Lisbon, Portugal*
- [238] Bertin J J and Cummings R M 2003 *Progress in Aerospace Sciences* **39** 511–516
- [239] 2006 *Proceedings of the Fifth Workshop of Thermal Protection Systems and Hot Structures, Noordwijk (The Netherlands) ESA SP-631*
- [240] Armenise I, Capitelli M, Gorse C, Cacciatore M and Rutigliano M 2000 *Journal of Spacecraft and Rockets* **37** 318–323
- [241] Billing G D 2000 *Dynamics of Molecule Surface Interaction* (Wiley)
- [242] Cacciatore M and Billing G D 1990 *Surface Science* **232** 35–50
- [243] Arasa C, Busnengo H F, Salin A and Sayós R 2008 *Surface Science* **602** 975–985
- [244] Sayós R, Morón V, Arasa C and Busnengo H F 2009 *Proceedings of the Sixth European*

- Symposium on Aerothermodynamics for Space Vehicles, Versailles (France) ESA SP-659*
- [245] Bedra L and Balat-Pichelin M 2005 *Aerospace Science and Technology* **9** 318–328
- [246] Berkut V D, Doroshenko V M, Kovtun V V, Koudryavtsev N N, Novikov S S, Smirnov N V and Sharotovov A I 1992 *Soviet Journal of Chemical Physics* **9** 2222–2237
- [247] Gamallo P, Rutigliano M, Orlandini S, Cacciatore M and Sayós R 2012 *AIP Conference Proceedings* **1501** 1129–1136
- [248] Morón V, Gamallo P and Sayós R 2011 *Theoretical Chemistry Accounts* **128** 683–694
- [249] Morón V, Martin-Gondre L, Crespos C, Larregaray P, Gamallo P and Sayós R 2012 *Computational and Theoretical Chemistry, Special Issue Chemical reactivity, from accurate theories to simple models, in honor of Professor Jean-Claude Rayez* **990** 132–143
- [250] Morón V, Martin-Gondre L, Gamallo P and Sayós R 2012 *The Journal of Physical Chemistry C* **116** 21482–21488
- [251] Sepka S, Chen Y K, Marschall J and Copeland R A 2000 *Journal of Thermophysics and Heat Transfer* **14** 45–52